VISUALIZATION OF NUCLEAR TARGETING OF BREAST CANCER CELL LINES

and

QUANTIFICATION AND DETECTION OF MATRILYSIN PRODUCED BY FIVE CANCER CELL LINES

By

Daniel Charles Dorset

Thesis

Submitted to the Faculty of the

Graduate School of Vanderbilt University

in partial fulfillment of the requirements

for the degree of

MASTER OF SCIENCE

in

Biomedical Engineering

December, 2006

Nashville, Tennessee

Approved:

Todd Donald Giorgio

Frederick R. Haselton

ACKNOWLEDGEMENTS

This work was made possible by grants from the Department of Defense. I am especially indebted to Dr. Todd Giorgio, Dr. Rick Haselton, and Dr. Oliver McIntyre for their time guidance, and support. I would also like to thank the intracellular lab members, past and present, who familiarized me with the lab and its equipment and lent me their expertise: Dr. Sam Kuhn, Dr. Adam Smith, Chinmay Soman, Ashley Aston-Weiner, Chris Pino, Ash Jayagopal, Dr. Tricia Russ, Dr. Greg Stone, and Elizabeth Dworska. Dr. Van Saun of the Matrisian lab and Sedef Everest from the McIntyre lab also provided Western blot assistance and cell lines, respectively.

My family has been and continues to be an endless fountain of love and support, without which I would have never reached this stage of my academic career.

TABLE OF CONTENTS

LIST OF TABLES

LIST OF FIGURES

CHAPTER I

RATIONALE AND SPECIFIC AIMS

Rationale

Cancer is currently estimated to account for 22.7% of all deaths in the United States, making it the second most common cause of death. In women between the ages of 40 and 79, cancer is the leading killer. Breast cancer is the second leading cause of cancer deaths in women, below lung cancer and above colon/rectal cancer. An estimated 212,920 new cases of breast cancer will be diagnosed in 2006. 40,970 women are expected to die from it in 2006. As with most other cancers, breast cancer mortality rates have been trending downward, but the number of new cases is still large. Current estimates predict that one in twelve women will develop breast cancer in her lifetime[40].

Campaigns touting breast cancer awareness and early detection have been instrumental in this downward trend. However, improving the reliability and ease to the patient and physician of early detection methods will encourage more Americans to seek early diagnosis and prevention of cancer. The likelihood of surviving any cancer is inversely proportional to the progress of that cancer upon its diagnosis and the initiation of treatment[52].

The identification of enzymes and other proteins secreted either exclusively by cancer cells or differentially relative to normal tissue cells is crucial to improving early detection methods. The ideal cancer marker will be detectable through reliable, non-invasive methods such as the analysis of saliva, sweat or urine. Barring that, minimally invasive methods such as blood sampling or the administration of a detection agent that could passively detect

malignant activity and even give location information would be a significant improvement as well[20].

There are few reliable cures for cancer, and any increase in effectiveness will likely require tailoring to the individual case based on the patient, cancer location, cancer stage, and other factors. The development of quick, reliable, means of targeting specific types of malignant cells will be an important step to personalized cancer treatment. There exists a wealth of ideas on this front, many of which are currently in the conceptual and experimental stages. Proof of a therapeutic approach's effectiveness by experimentation is a crucial step towards clinical acceptance of the approach.

Specific Aims

Approximately half of the work in this thesis is dedicated to measuring production of matrilysin by five human cell lines isolated from benign and malignant breast and colon tumors. Specific knowledge of matrilysin production capabilities will allow precise configuration of therapies targeting colon, breast, and other tumors that employ the action of the enzyme. The methods used in this experiment can also be carried over to studies of other proteases, provided that sufficient detection measures are available.

In her master's thesis, Ashley Aston-Weiner described a method by which she used phage display to isolate a heptamer peptide fusion displayed on the pIII coat of M13 that would allow the phage to enter the breast cancer cell lines MCF-7 and MCF10A and locate to their nuclei. She found several sequences associated with nuclear-localized phage, one of which was Gln-Pro-Ser-Pro-Ser-Pro-Thr (QPSPSPT). While she provided evidence of their nuclear targeting ability by amplifying the phage recovered from isolated nuclei, she experienced difficulty in visually verifying the process[95]. The other

half of this thesis describes this phase of the project: the visual verification of nuclear-targeting function of M13 bacteriophage using direct fluorochrome labeling and detection with nuclear staining and subsequent fluorescence microscopy.

CHAPTER II

MANUSCRIPT 1: VISUALIZATION OF PHAGE LOCALIZATION

Introduction

Gene Therapy – From Theory to Laboratory

The world of genetics sprang to the forefront of the public scientific consciousness during the biotechnology revolution of the 1990s. At the helm of this explosion of popularity sat gene therapy, bolstered by its promise of being able to cure any ailment that had a genetic basis, and perhaps some that didn't. Kary Mullis' discovery of the Polymerase Chain Reaction which allowed simple, cheap, specific, and quick mass replication of as little as a single strand of DNA opened up the field in 1988[58].

On paper, gene therapy is so simple as to be attractive to the layperson: first, a cloned gene is inserted into a genetic construct using molecular "scissors," restriction endonucleases. Next, the genetic construct is similarly spliced into the genome of a virus that has the ability to replicate engineered out of it, or the construct is attached to or inserted into a carrier. This virus or synthetic carrier acts as a vector to insert the viral genome with the therapeutic gene spliced in into the host cell genome or to deposit a plasmid cargo into the nucleus. The host cell then expresses the newly inserted gene, replacing the defective gene or producing a protein that will alleviate an undesired condition[70].

However, the realities of gene therapy's complexity were soon revealed. Viral vectors are frequently immunoreactive and thus decrease the possibility for repeated

administrations. The most familiar viral vector, the adenovirus, inserts a genetic construct that does not integrate into the host cell genome, thus causing a transient expression that is insufficient for replacing an undesired gene and therefore not an acceptable solution for long-term management of a genetic ailment[42].

Ideally, gene therapy permanently resolves a monogenic disorder by supplementing the defective gene with a corrected gene in a sufficient number of cells to remove most or all of the negative effects of the disorder. Many in the field also see potential for gene therapy in treating polygenic disorders, through the same method as above or by producing an auxiliary protein product that interacts with an undesired protein product to inactivate or counteract its negative effect. Another approach, still largely in the theoretical realm, is to "switch" a transfected gene on or off by administration of a particular medicine, or, even more conveniently, by conditional expression of a particular protein product. The eventual nuclear signaling that would occur as a response to the cell's detection of the protein or medicine could trigger the transcription of the transfected gene. For example, a cancer "vaccine" of sorts could be developed in which a large number of cells express the protein product of a transfected gene in response to the action of an enzyme or other protein product overexpressed by malignant cells[18].

The lessons and techniques learned through the many studies of gene therapy have resulted in its approaches being applied to animal modeling. Animal models, especially those created with mice, are a huge benefit to researchers studying the immune system and cancer, among other things. The ability of selective removal or conditional deactivation of a gene has led to many important discoveries of gene function, many of which can be assumed to have similar effects in their human orthologues. Knockout mice can be created by

selectively breeding or cutting out (by engineering) a desired gene or genes in the embryonic or stem cells of a mouse. Series of knockout mice can be used to discern the controlling factors and protein products involved in a particular pathway. Much understanding of the human genome and disease processes has been gained from animal modeling, and the field is currently very active, with hundreds of papers being published annually[5].

Gene Therapy Modalities

There are typically considered to be four types of viral gene therapy: adenoviruses, adeno-associated viruses, retroviruses, and other. As mentioned above, a frequent problem with the use of viral vectors is inflammation and immunoreactivity with subsequent treatments. However, when compared to the current non-viral methods, viral gene therapy more often results in efficient transfection of target cells.

Adenoviruses are a group of 26 known viruses that have approximately a 35 kilobase double-stranded DNA genome and can accommodate inserts of up to 2 kilobases; they are approximately 100 nm in diameter. Adenoviruses derive their name from their ability to cause mild respiratory tract infections in humans. Typical method of entry is through the coxsackie-adenovirus receptor (CAR), which binds to the adenovirus coat proteins and the $\alpha_v\beta_3$ integrins. The virus then enters the host cell via a clathrin coated pit. The viral genome replicates independently of the host cell's chromosomes. Numerous studies on adenoviruses for gene therapy have found that serotypes 2 and 5 are the most efficient for gene therapy, and deletion of the E1 gene prevents virus renewal. Adenoviruses have many significant advantages. High titers are reliably attainable, the viruses can infect both dividing and non-dividing cells, and the viruses can be covered with a co-polymer, which theoretically can

reduce their immunoreactivity by covering immunogenic surface proteins while still preserving vector function[12].

The major disadvantage of adenoviruses besides their capacity to elicit an immune response is that these vectors do not integrate into the host cell genome. This coupled with the sometimes-dangerous immune response created by the virus's presence makes attempted transfection of a therapeutic gene transient at best, and a toxic failure at worst. Problems of immunogenicity and packaging limits are currently being addressed with "gutless" adenoviruses, which use a helper adenovirus in a tissue culture to obtain the proteins necessary to infect human cells without having to possess the DNA that codes for them. While this new technology is encouraging, it does not meet the challenges of versatile or long-term expression, and contamination of the gutless adenovirus titer with helper virus is still a problem that prevents its advancement into clinical trials[17].

Adeno-associated viruses are small parvoviruses which got their name from their discovery as a contaminant of adenovirus cultures. They are much smaller than adenoviruses, having a diameter between 18 and 26 nm and weighing between 5.5 and 6.2 megadaltons. Adeno-associated viruses posses a single-stranded DNA genome of approximately 4.7 kilobases (this genome must be cut down to 4.4 kilobases for gene therapy purposes) and are not pathogenic. In order to replicate, they

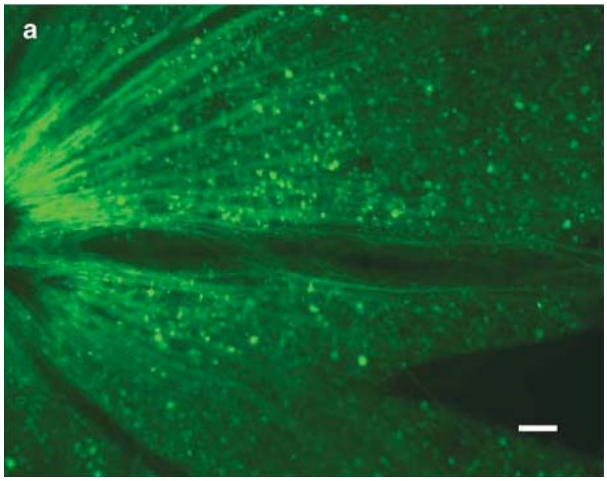

Figure 1: Specific transfection of retinal ganglion cells with a green fluorescent protein gene using an adeno-associated viral vector. Note the clear path of the axons[1].

require the host cell to be infected by another virus, usually an adenovirus or herpes-family virus. However, in the absence of these "helper viruses," adeno-associated viruses are in a latent phase, where they integrate their genome into the host cell's genome. Once inside the host cell, the protein portions of the virus are quickly broken down. It is this latent phase that makes adeno-associated viruses so attractive for gene therapy[77].

By integrating their genome with that of the host cell without undergoing replication, the virus can avoid eliciting an immune response while sustaining long-term expression. Adeno-associated viruses infect both dividing and non-dividing cells, making them especially attractive for infecting the retina. Furthermore, the virus enters the cell by binding to heparin sulfate proteoglycans, which are exposed on a broad range of cells. While adeno-associated viruses are currently the most successfully employed viral vectors for gene therapy, they cannot accommodate large inserts because of their 4.4 kilobase limit. Of the known adeno-associated virus serotypes, number 5 is currently considered to be the safest and most efficient[88].

Retroviruses are a family of viruses with an enveloped single-stranded RNA genome. Important genera include oncovirinae, lentivirinae, and spumavirinae[67]. Retroviruses get their name from the fact that they must use the enzyme reverse transcriptase to transcribe their RNA genome into a DNA genome inside the host cell. Retroviruses currently possess several disadvantages that currently make them unattractive for use as gene therapy vectors, but they have some interesting properties that could be exploited. Retroviruses require breakdown of the nuclear envelope in order to integrate their genome into that of the host cell, which means they only infect dividing cells. The probability of reversion of an engineered retrovirus to its wild-type form by interaction with "helper cells" is a significant

risk when using these vectors. However, retroviruses can obtain high titers and can accommodate up to 7.5 kilobases of foreign DNA. An interesting feature of retroviruses is that they can somehow absorb other viral proteins, potentially giving engineers the ability to introduce novel or known targeting proteins into the retrovirus coat that would allow targeting of specific cell types, a process known as "pseudotyping." [54]

Lentiviruses are a genus of retrovirus which have added advantages as well as added disadvantages. Unlike typical retroviruses, lentiviruses can infect non-dividing cells. Long term expression of transfected genes delivered via lentiviruses has been shown[17]. However, the only lentivirus currently being studied for gene therapy is a highly modified form of the human immunodeficiency virus (HIV). Because of the aforementioned risk of wild-type reversion by recombination, there is always some risk in using modified HIV as a vector in humans. Thus, there are currently no clinical trials in progress using this vector, but its ability to efficiently transfect human cells, including corneal epithelial cells, has been shown in animal models. Therefore, lentiviruses could become useful to humans in the future or in gene therapy of animals.

Many examples of non-viral gene therapy have been conceived over the years, a great deal of which have been abandoned, but there remain several that are still heavily studied[5]. These multiple dead-ends that researchers encountered with viral delivery methods led many to consider non-viral methods, ranging from the "gene gun[7]" to the biomimetic liposome-DNA complex[4] to simply "naked DNA.[43]" A major issue with all non-viral methods is that they employ plasmids rather than a genomic integration approach. A major reason for this is the inability to target these vectors to the nucleus in a non-cytotoxic manner. The main limiting factor in non-viral gene therapy is the ability to get DNA, be it in plasmid or loose-

strand form, to the nucleus of a cell once the non-viral transport construct has entered the cytoplasm.

Non-viral vectors can be divided into two broad categories: physical and chemical. Most physical methods include mechanical, electrical, and surgical modes of transduction. The aforementioned "gene gun" would be an example of a mechanical method – using force to push a plasmid attached to a gold nanoparticle through the cell membrane. While the DNA-containing construct often enters the cell successfully, nuclear damage can occur and the efficiency and specificity are poor. Electroporation uses a quick jolt of electricity to reversibly permeabilize the cell membrane. This can be done reliably without inflammation or significant damage occurring, but since the DNA is in the form of a plasmid, any expression will be transient. A promising surgical method is to use carbon nanotubes coated with a protective carbohydrate as a syringe to safely pierce the cell membrane and deliver a plasmid to the cell nucleus. Carbon nanotubes can also be functionalized with a positively charged ion such as ammonium that will allow DNA to attach. These nontoxic nanotube-DNA complexes can then passively enter the cell[26].

The chemical category of non-viral vectors is a somewhat abstract definition, as most physical methods require chemical ligations to achieve their ends. Thus, chemical methods can be used either alone or to supplement other gene therapy modalities. Fort example, high salt solutions or environments containing polycations can improve transduction. This is currently only feasible for *ex vivo* or *in vitro* transfections. The major chemical method currently being pursued is the development of liposomes. At their simplest, these constructs are simply lipid bilayer spheres that contain DNA. However, their use in gene therapy can be enhanced by using cationic lipids and functionalizing the liposomes with targeting proteins

such as viral peptides or antibody variable regions[4]. While some nonviral vectors are promising, others are obvious dead ends. The major disadvantage with the current crop of non-viral vectors is that they all employ plasmids, which obviates their potential for causing long-term expression of the therapeutic gene. With all of the non-viral methods studied so far, *in vivo* transfection has not been performed with acceptable efficiency or permanent expression.

While gene therapy has mostly vanished from mass market periodicals and been replaced by proteomics at the top of the syllabi of introductory biotechnology courses, it remains a heavily researched field, albeit one with less frequent dramatic breakthroughs. The hunt for the "ideal vector" is still in progress, and many believe its discovery, should it come, will be the "second wind" for the field. This ideal vector will be safe (non-immunogenic with a low risk of insertional mutagenesis), relatively cheap to mass-produce, be easily customizable to target a wide variety of cells in a significant majority of patients, possess long-term expression and stability, and have a high capacity for therapeutic DNA, allowing it to fix genes of any biologically relevant length. Whether or not gene therapy will one day be the answer to the majority of humanity's ailments is an answer that is still waiting in the wings, but its potential still shines bright in the eyes of many scientists and engineers[12].

M13 Bacteriophage

M13 is one of a group of filamentous bacteriophages, so named because of their proportions. A single typical M13 virion is approximately 6.5 nm in diameter and is 930 nm long, giving it the proportions of a "four foot long pencil." M13 has several coat proteins; the ones of interest to the project are pVIII and pIII. The M13 virion has

approximately 2,700 copies of the pVIII protein on its surface, but only 5 copies of the pIII coat protein, all of which are concentrated at one end of the virion. Despite their reduced number, the pIII coat proteins are responsible for binding to the F-pilus of *E. Coli*[37].

Upon phage binding, the pilus retracts, pulling the phage towards the bacterium. The N1 domain of the pIII phage protein interacts with the TolA protein on the bacterium membrane, facilitating phage DNA entry. Once inside the bacterium, the single-stranded DNA of the phage is transcribed to its double-stranded form, and select proteins from the phage amplify this transcript, and more phages are produced. M13 is a non-lytic phage—it does not kill the host bacterium. However, the host bacterium's division rate is reduced by approximately one-half[69].

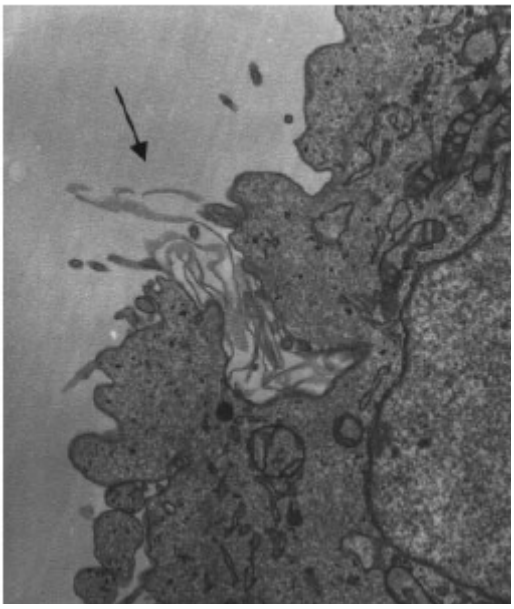

Figure 2: Electron micrograph of M13 bacteriophages (black arrow) entering a HeLa cell[27].

While bacteriophages only reproduce in bacteria, they have been shown to enter eukaryotic cells. A study by Giovine et al. goes into detail on the method of cell entry by phages[27]. In their experiment, they engineered M13 bacteriophages to display an adenovirus peptide that facilitated cellular entry. The paper contained several excellent electron micrographs depicting phage entry into eukaryotic cells, and the pictures indicate that it is a combination of membrane protein interaction and pinocytosis (Figure 2).

Phage Display

Phage display is an indirect method of genetic engineering in which random peptides displayed on the coat proteins of bacteriophage are detected and classified by a selection or screen. Phages of interest are amplified in *E. coli*, and phage DNA is sequenced and analyzed to discover the sequence of the peptide of interest. Phage display is commonly employed as a low-cost method to discover novel antibody binding motifs, but more elaborate uses for it have been discovered as well. For example, insertion of random sequences followed by a linker domain can be used to detect protease substrates. Phages displaying certain ligands have been shown to act as seeds in the formation of silver nanocrystals[37].

Nuclear Entry

Separating the nucleus from cytoplasm in non-dividing cells is the nuclear envelope, consisting of a phospholipid bilayer and various proteins, including pores formed by nuclear pore complexes. These pores regulate passage of cytoplasmic objects through the nuclear envelope. Passage through the nuclear pore complex can be either a passive or an active process. Besides ions and small compounds, compact proteins up to approximately 60 kDa can diffuse through the complex. Large proteins and protein-nucleic acid complexes are selectively transported into and out of the nucleus, and must interact with the transporter proteins of the nuclear pore complex[46].

A "nuclear localization sequence" is required in order for a protein to be transported through the complex. The first nuclear localization sequence to be characterized was in the large-T antigen of the simian virus 40. A seven-peptide, highly-

basic, highly hydrophilic region, PKKKRKV, was identified as the nuclear localization sequence for the virus. Other nuclear localization sequences have been identified since then, and some have different chemical properties, such as high hydrophobicity[29].

Four required proteins have been identified in the active nuclear import process: Ran, NTF2, and the importins α and β. Briefly, the importins form a complex, with the α subunit binding to the nuclear localization sequence of a cargo protein, and the β subunit interacting with the FG-nucleoporins of the nuclear pore complex. The FG nucleoporins are so named because of their hydrophobic regions of repeated phenyalanine (F) and glycine (G) residues. Other homologs to importin β have been identified that interact with various nuclear localization sequences directly to facilitate nuclear entry.

Ran is a guanine-binding protein that serves as an "escort protein" to a cargo-bound importin complex. The cargo-bound importin and Ran-GDP complex interacts with the FG-nucleoporins in a successive fashion, eventually passing through into the nuceloplasm. Once inside the nucleus, Ran-GTP interacts with the importin complex, causing a conformational change that releases the cargo. Ran-GTP then escorts the unbound importin heterodimer back into the cytoplasm[46].

Project Purpose

The goal of this project was to demonstrate entry and nuclear localization of M13 phage bearing a heptamer peptide into eukaryotic cells in culture. Visualization was achieved using amine-reactive fluorochromes that can be directly conjugated to the abundant pVII surface coat proteins of the phages. Evidence of the peptide's capability to confer

nuclear localization potential to a bacteriophage will justify further examination of the peptide and the methods used in the peptide's discovery.

Ashley Aston-Weiner's previous work isolated a sequence that localized to the nuclei of both MCF-7 and MCF10A cells. She used a phage display library (Ph.D.-7, New England Biolabs, E8100S) to generate a wide variety of phages displaying different heptamer peptides on their pIII coat proteins. The phages were incubated with MCF-7 and MCF10A cells overnight, and then the nuclei of the cells were isolated. Phages associated with the isolated nuclei were recovered, amplified, and sequenced to determine the possible peptide sequences that conferred the potential for nuclear localization. The sequence QPSPSPST was frequently displayed by phages rescued from the nuclei of both cell lines.

In the same project, visualization of phage localization was also attempted using immunohistochemistry methods. The need for antibody entry into the cell—and presumably, the nucleus—significantly complicated the permeabilization approach. Incomplete and/or variable permeabilization complicated interpretation of the IHC in assessing the location of the phage. Therefore, in regards to visually verifying the intracellular localization of phage, immunohistochemistry is not sufficient. A different strategy was necessary—one that allowed the phage to be labeled prior to incubation with cultured cells. The detection method also required that the label be detectable without permeabilizing the cells. A literature search revealed a novel technique for directly labeling the pVIII coat protein of an M13 bacteriophage with an amine reactive succinimidyl ester such as the Alexa Fluor line of fluorochromes.

Materials and Methods

Phage Labeling

As described in Jaye, et al. 2001[39], phage suspension initially at 4º or -86º C and mixed 1:1 with 100% glycerol containing on the order of 10^{13} plaque forming units (determined by titer), was added to microfuge tubes (Sigma, Z666505) along with ¼ volume of sterile 20% polyethylene glycol-8000 (Sigma P413) and 2.5M NaCl (Fisher, S603-4) precipitation buffer. The mixture was vortexed and maintained at 4º C for at least four hours before centrifuging at 4º C, 20,000 RCF for 20 minutes in a microcentrifuge (Eppendorf, Z2413-R). The supernatant was discarded, and 5 µL of 5% w/v Alexa Fluor 647 in dimethyl sulfoxide (DMSO) were added to the tubes of phage for labeling. 95 µL of 1 M $NaHCO_3$ conjugation buffer were then added to each tube. Tubes were placed in the dark for one hour, with vortexing every 15 minutes. After the conjugation period, 200 µL of precipitation buffer were added to each tube and the tubes were placed at 4º C for at least one hour. All tubes

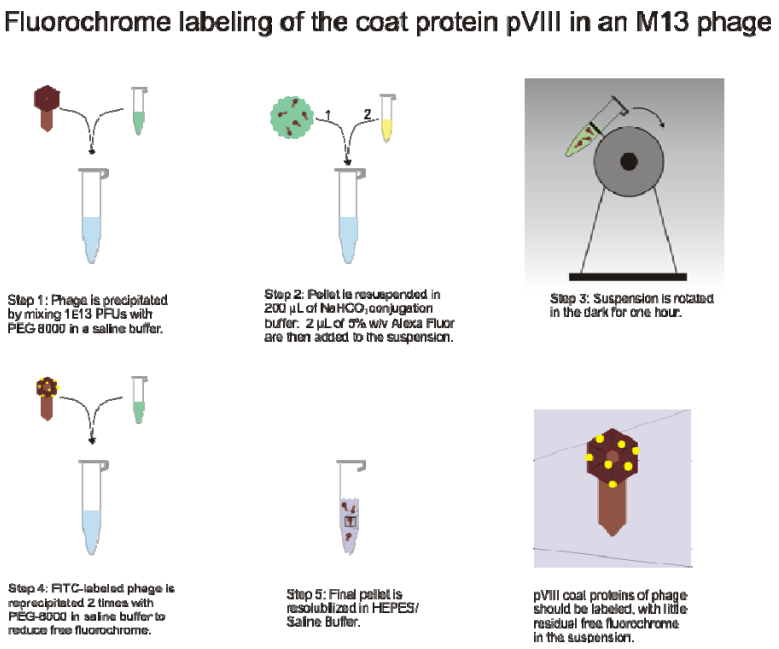

Figure 3: Schematic depicting fluorochrome-labeling process for M13 bacteriophages.

were then centrifuged at 4º C, 20,000 RCF for 15 minutes, and the supernatant was discarded.

200 µL of precipitation buffer was once again added, and the tubes were placed at 4º C for at least one hour before centrifugation at the same conditions as before. This step was repeated once more and then the phages were resuspended in 100 µL of a 100 mM NaCl, 10 mM HEPES, ph 7.9 suspension buffer. To ensure a lack of free fluorochrome in the final labeled phage suspension, supernatants were collected after washings and analyzed using a Nanodrop Spectrophotometer (ND-1000, Nanodrop Inc.) calibrated to detect Alexa Fluor 647 at its optimal excitation and emission wavelengths.

As a negative control, the above process was performed without the addition of fluorochrome and DMSO to the negative control tubes.

Phage Agglomerate Sizing and Filtration

Samples of labeled and unlabeled phages that had gone through the steps of the above procedure were diluted to 200 µL (~10^{13} PFU) in suspension buffer and pipetted into clean cuvettes suitable for use in the Zetasizer Nano ZS particle measuring device (Malvern). Particle size distributions were assessed using both continuous and discrete modes. Raw data obtained by the Malvern DTS companion software program were exported to tab-delimited format for use in Excel and SigmaStat. Phage agglomerates greater than 5.0 µm in diameter were filtered out of suspension using Ultrafree PVDF centrifugal filtration devices (Millipore, UFC40SV25). The filtrate was harvested, its particle size distribution was reassessed again, and the remainder was collected for use in the phage incubation and staining, as described below.

Phage Incubation and Cell Staining

Approximately 10^3 cells were added to each well of a 12-well plate with 1 mL of OptiMEM reduced serum media and allowed to adhere for 8 hours. Approximately 10^{10} plaque forming units of labeled or unlabeled, targeted or untargeted phage were added to the appropriate wells. The plate was placed on a shaker in a 37º C incubator overnight. The next morning, the wells were aspirated and washed thrice with Ca^{2+}, Mg^{2+} free PBS (CMF-PBS) (Sigma, P-4417) and 500 μL of 3.7% paraformaldehyde was added to each well for 30 minutes. The wells were washed thrice with CMF-PBS, and 900 μL of 300 nM DAPI in Ca^{2+}, Mg^{2+} free PBS was added to each well for 5-7 minutes. The wells were once again washed thrice with CMF-PBS, 500 μL of fresh CMF-PBS were added to each well, and the cells were observed under a fluorescent microscope.

Nuclear Visualization

Cells were observed with a Nikon Eclipse TE2000-U fluorescent microscope with Hammamatsu CCD attachment. Although the camera was capable of color image capture, all photos were taken in 8-bit grayscale to make the image files readable on other computers. Cell nuclei stained with DAPI were visualized with a Nikon DAPI-FITC-Texas Red triple cube filter (Nikon, 96356), while a Cy5 filter (Nikon, 96758) was used to visualize the Alexa Fluor-labeled phages. Typical exposure time for visualizing DAPI stained nuclei was 200 msec, while exposure time was up to 5 seconds for phage visualization. Exposure times were significantly less for phages labeled with Alexa Fluor 488. Original captured images were stored unmodified in 8-bit grayscale TIFF format in order to be available for later analysis.

Image Processing

Due to the limitation of the ImagePro 5.0 software used to take pictures from the fluorescent microscope, photographs had to be taken in 8-bit grayscale. Images were colored and combined in Corel PhotoPaint 12, and the processed images were stored in PNG format. 8-bit grayscale TIFFs created by the ImagePro 5.0 software from triple cube filter photographs were converted to blue, while the Cy5 filter photographs were converted to red. FITC filter photographs were converted to green. The Cy5/FITC photographs were placed over the DAPI photographs of the same frame, and the black pixels were removed using the Color Transparency algorithm. Remaining pixels were outlined by the program, and circles were drawn around red clusters larger than 3 pixels. These photographs were exported to PNG or JPG format, and some were combined with phase contrast photographs using the same transparency algorithm. A 1:1 scale was maintained during each manipulation to minimize image processing artifacts. The original files were also saved in order to ensure the integrity of future follow-up analyses.

Details of the experiment used to generate photographs from 9th May and 12th May:

In each of six 1.5 mL microfuge tubes, 200 µL of QPSPSPT-displaying phages (approximately 2E13 Plaque Forming Units) were combined with 50 µL of precipitation buffer. Tubes were refrigerated for at least one hour at 4º C and then centrifuged at 20,000 RPM, 4º C for 15 minutes. Pellets were resuspended in 200 µL of conjugation buffer, and Alexa Fluor 488 was added to each tube in increasing amounts—0.25, 0.5, 0.75, 1.0, 1.5, or 2.0 µL. The tubes were incubated for one hour in the dark at room temperature and vortexed

every 15 minutes. 50 μL of precipitation buffer were added to each tube, and the tubes were maintained at 4º C for at least one hour. The labeled phages were washed twice with 200 μL of precipitation buffer to eliminate free-fluorochrome, and the washed pellets were resolubilized in 200 μL of HEPES/NaCl suspension buffer and maintained in the dark at 4º C until ready for use.

MCF-7 and MCF10A cells were subcultured and dispensed into each well of a separate 24 well plate with a seeding density of 5000 cells/well. The cells were allowed to attach and grow in serum-containing media (see Appendix A) for 24 hours. Three of the four wells in a column of the 24 well plate received up to 10 μL (approximately 10^{12} PFU) of phages from one of the six tubes of phages labeled in varying concentrations of flurochrome. The fourth well received no phages and served as an autofluorescence control to determine if any autofluorescence was present. After addition of phages, the plates were incubated overnight (~16 hours) in standard cell culture conditions.

After the incubation period, each well was washed twice with 500 μL of calcium and magnesium-free PBS (CMF-PBS). 500 μL of 3.7% paraformaldehyde were then added to each well, and the plates were maintained at 4º C for 20 minutes. Each well was then washed twice with CMF-PBS and the cell nuclei were stained with 300 nM DAPI for ten minutes. The wells were then washed twice with CMF-PBS to remove free DAPI. 500 μL of CMF-PBS were added to each well, and the plates were covered and maintained at 4º C until time for viewing.

Combined Serum-Free Medium + Transport Mechanism 24-Well Plate Experiments

All wells of a 24-well plate were seeded with 5000 cells of either MCF10A or MCF-7 cell lines, according to the diagram in Figure 4. Cells in all wells were allowed to grow in 300 µL of normal growth medium (containing fetal bovine serum) at standard culture conditions for at least 24 hours. After the growth period, growth medium was aspirated from wells in rows marked "SFM" (serum-free medium) in the diagram in Figure 4, and the media in these wells was replaced with 300 µL of serum-free medium. Phages were then added to the wells in rows labeled "Standard" in microliter amounts corresponding to the numbers in the circles in Figure 4.

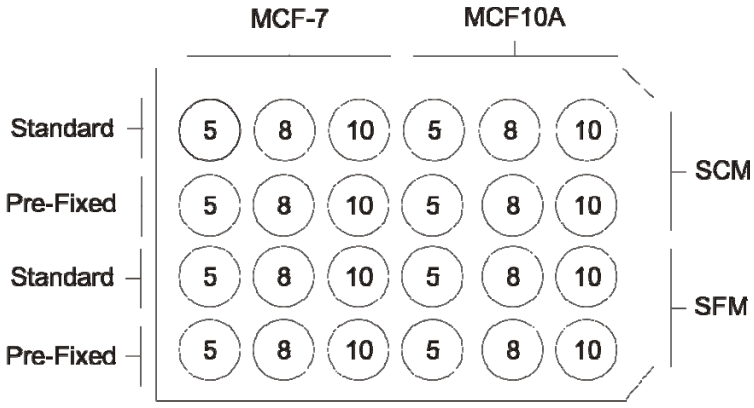

Figure 4: Schematic of 24-well plate experimental setup. The numbers in each circle denote the volume of labeled phage added to each well, in microliters. 1 µL of phage is ~10^{10}PFUs.

The cells were incubated with the phages overnight in standard cell culture and conditions. The next day, cells in all wells were fixed, and their nuclei were stained as described in the "Phage Incubation and Cell Staining" section. Cells in the "standard" wells were examined by fluorescence microscopy, and areas of interest were photographed. Then, phages were added to the wells in rows labeled "Pre-Fixed" in microliter amounts corresponding to the numbers in the circles in Figure 4. The plate was then incubated overnight in standard cell culture conditions. The next day, the wells in the "pre-fixed" rows were washed thrice with CMF-PBS and then received 300 µL each of fresh CMF-PBS. Wells were then examined using fluorescence microscopy.

Phage DNA Extraction and Sequencing

Phage DNA was extracted using the QIAPrep Spin M13 Kit (Qiagen, 27704) as directed by the manufacturer. Briefly, 700 μL (~3 * 10^{15} PFU) of amplified phage suspension were combined with 7 μL of the precipitation buffer provided in the kit and loaded into a spin column. The suspension was vortexed and maintained at room temperature for 2 minutes, and then the suspension was centrifuged at 8000 RPM for 15 seconds. Filtrate was discarded, and 0.7 mL of phage lysis buffer were added to the spin column. After discarding the filtrate, the column was immediately centrifuged at 8000 RPM for 15 seconds, filtrate was discarded, and then 0.7 mL more of phage lysis buffer were added to the column. The column was left in room temperature for 1 minute and then centrifuged at 8000 RPM for 15 seconds.

Filtrate was discarded, and buffer PE (provided in the Qiagen kit) was added to the column to remove residual salt from the lysis process, and the column was centrifuged at 8000 RPM for 15 seconds. Flow through was discarded, and the spin column was inserted into a fresh 1.5 mL collection tube. 100 mL of DNA elution buffer provided in the kit were added directly to the spin column membrane, and the spin column was allowed to sit for 10 minutes at room temperature. The column was then centrifuged at 8000 RPM for 30 seconds. The filtrate was capped and stored at 4º C until sequencing. The DNA was sequenced using the g96III primer included in the New England Biolabs Ph.D.-7 Phage Display Peptide Library Kit (New England Biolabs, #E8100S) in the Vanderbilt DNA Sequencing Facility.

Results

Nuclear Targeting with Phage

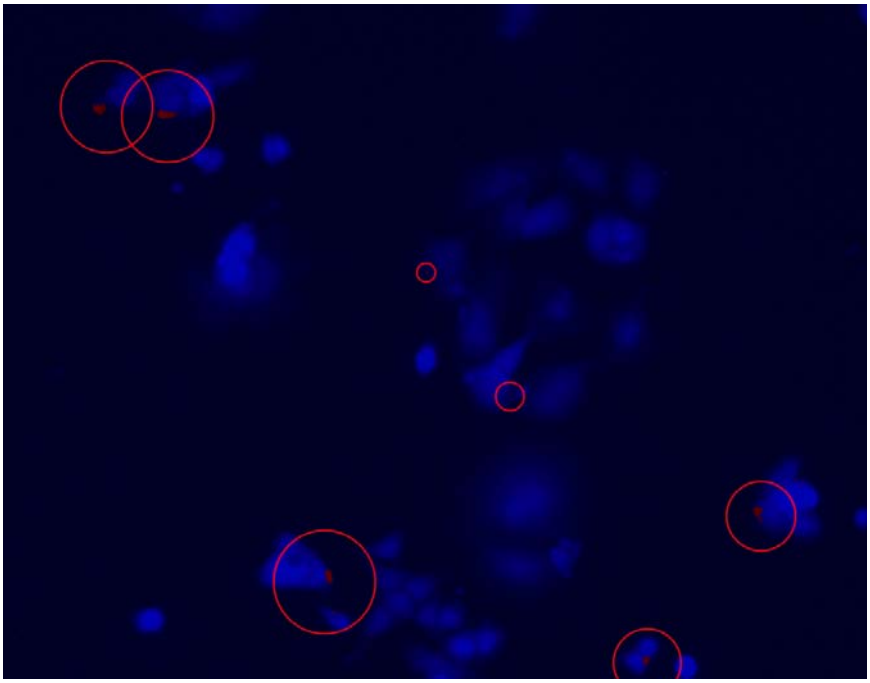

Figure 5: Bacteriophages displaying the QPSPSPT peptide labeled with Alexa Fluor 647 (red) are localized to the DAPI-stained nuclei of MCF-7 cells (blue) following 18 hours of incubation.

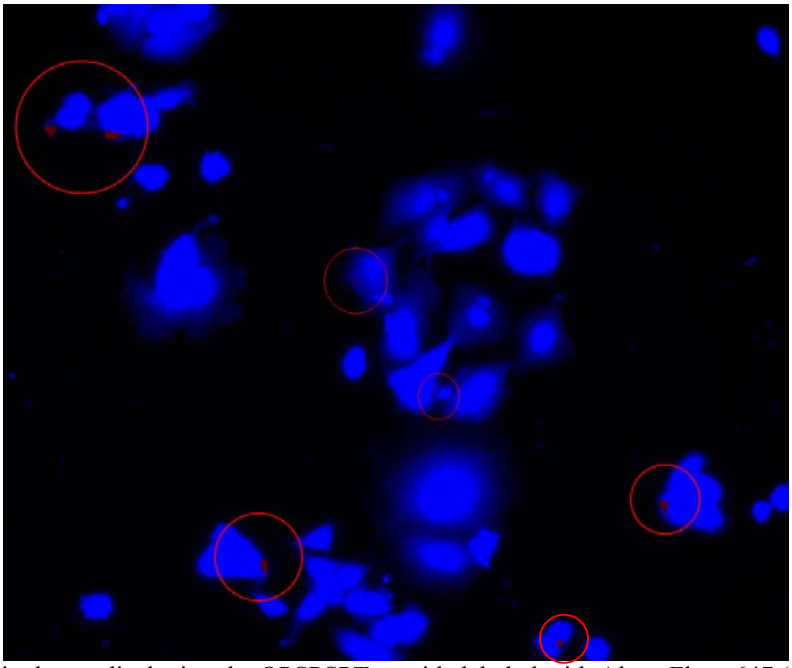

Figure 6: Bacteriophages displaying the QPSPSPT peptide labeled with Alexa Fluor 647 (red) are localized to the DAPI-stained nuclei of MCF10A cells (blue) following 18 hours of incubation.

The first fluorochrome chosen was Alexa Fluor 647. The maximum excitation wavelength for this fluorochrome is 647 nm, with a maximum emission wavelength of 667 nm. This wavelength is difficult to see with the unaided eye in the fluorescence microscope. Display of this color using the imaging and visualization tools attached to the fluorescent microscope is also difficult to resolve by unaided vision. Thus, another fluorochrome was chosen: Alexa Fluor 488, with a maximum excitation wavelength of 488 nm and maximum emission wavelength of 520 nm, provides a green fluorescence compatible with robust visual detection. Conveniently, with a triple cube fluorescence microscope filter, both the excited fluorochrome and DAPI-stained nuclei could be identified simultaneously, allowing quick verification of phage localization to cell nuclei.

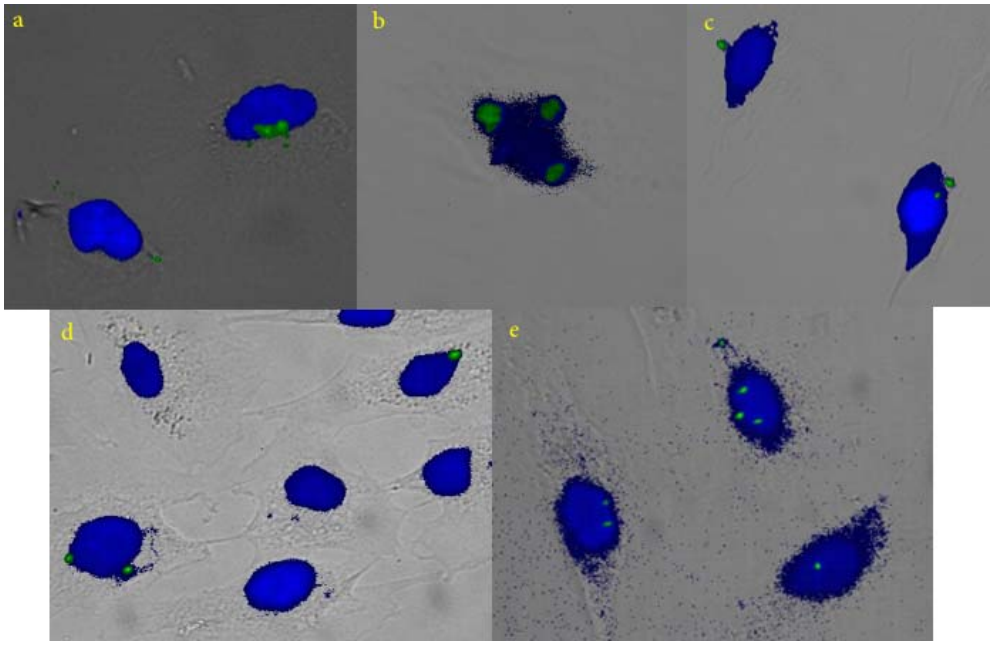

Figure 7: Bacteriophages displaying the QPSPSPT peptide labeled with Alexa Fluor 488 (green) are localized to the DAPI-stained nuclei of MCF10A cells (blue) after 18 hours of incubation.

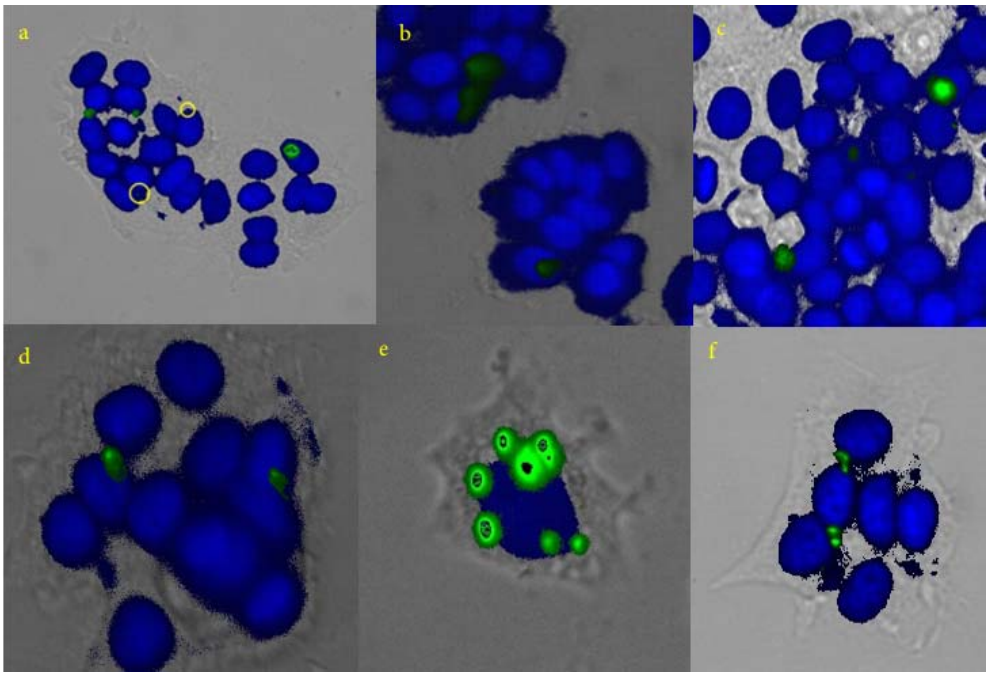

Figure 8: Bacteriophages displaying the QPSPSPT peptide labeled with Alexa Fluor 488 (green) are localized to the DAPI-stained nuclei of MCF-7 cells (blue) after 18 hours of incubation. Yellow circles in (a) denote faint phage spots.

Photographs were obtained that revealed preferential intranuclear and perinuclear localization of fluorochrome-labeled phage in MCF-7 and MCF10A cells (Figures 5-8). Combining the DAPI and phage filter photographs with phase contrast photos of the cells indicated that perinuclear phage localization was within the cell, but did not overlap the DAPI-stained nucleus. Further controls using phage that were fluorescently labeled but did not display the nuclear targeting peptide failed to demonstrate intracellular or nuclear localization.

The fields were analyzed, and the total number of phage spots, the total number of stained nuclei, the total number of nuclei bearing at least one phage spot, and the number of extracellular phage spots were counted. Based on the data obtained from the fields, it was estimated that the QPSPSPT-diplaying phages localized to 12.2% of MCF-7 cell nuclei, and to 34.2% of MCF10A cell nuclei. 4.5% and 4.8% of the phage spots were located extracellularly in the MCF-7 and MCF10A fields, respectively

After a thorough search, no areas of interest were noticed in the wells in which phages had been added after the cells had been fixed and stained.

Phage Labeling

Table 1: Fluorescence readings of free fluorochrome in successive washes after completion of phage labeling. Units are relative and arbitrary.

Average Phage Wash 1:	(88.4 +/- 0.7) * 10^3
Average Phage Wash 2:	(20.0 +/- 1.0) * 10^3
Average Phage Wash 3:	280 +/- 5
Average Control Wash:	20.7 +/- 38.0

Residual fluorescence was reduced to approximately the level of fluor-free control after three washes. Unconjugated Alexa Fluor was removed to minimize artifacts from cellular uptake of free fluorochrome not associated with phages.

DNA Sequencing

Phage DNA was sequenced at the Vanderbilt DNA Sequencing Facility after amplification of phages. By inspection of the data, the portion of the coding strand which coded for the heptamer peptide was isolated. The coding portion of the sequence was CAG CCT TCG CCT TCT CCT ACG. By comparison to a reverse codon table, the heptamer peptide Gln-Pro-Ser-Pro-Ser-Pro-Thr (one letter code: QPSPSPT) was confirmed. The complete sequence is shown in Appendix B.

Discussion

Fluorescently labeled M13 bacteriophage displaying the QPSPSPT peptide preferentially localized to the nuclei of MCF-7 and MCF10A cells in culture. Nonnuclear localization was not observed in fluorescently labeled phages lacking display of the heptamer peptide. Visualization of the intracellular localization of phage expressing the heptamer peptide on its pIII coat protein was an important verification step in the process of isolating and characterizing a novel nuclear localization sequence. Fluorescence microscopy and subsequent imaging processing provided a precise method of localizing two-dimensional phage position in the cell. Furthermore, phage internalization only occurs in live cells and requires an incubation period greater than one hour. The failure of phage to enter fixed cells supports phage cell entry as an active cellular process.

The frequency of observed nuclear interaction was estimated to be 12.2% and 34.2% for MCF-7 and MCF10A cells, respectively. A high frequency of nuclear localization is desirable in order for the peptide to be functional in gene therapy. However, there is a possible limiting factor based on the detection equipment. Individual phage particles might be difficult to detect using fluorescence microscopy, especially if a phage has fewer fluorochrome labels. It is possible that many of the nuclei only have a few labeled phages associated with them, making detection by fluorescence microscopy difficult. Furthermore, quantitative, statistical analysis of phage nuclear localization using fluorescence microscopy is difficult because of the thousands of cells in each well.

There could be more phage-nucleus interaction occurring than fluorescence microscopy could detect. Flow cytometry would be a better solution for future quantitative work but would likely require the difficult step of nuclear isolation. The

incubation period could also be varied. A 16-hour incubation period was standard, but it is possible that the results could change if different incubation periods are used.

A significant portion of the intracellular phage is observed at the borders of the stained nuclei. A possible explanation for this is that the phage is interacting with the nuclear envelope. Furthermore, aggregates of labeled phage would be less likely to enter the nuclei than unaggregated phage. Isolated, fluorochrome-labeled phage would likely be difficult or impossible to see with fluorescence microscopy. DAPI is an intercalating dye; it binds to grooves in double-stranded DNA. Thus, it is likely that the outer portions of the nucleus, which contain the nuclear membrane and pore complexes, are left unstained by the dye.

It is possible that over the incubation interval, many of the phages and their attached fluorochromes are destroyed by the cell endosomes. Perhaps only the fluorochromes or their fluorescence properties are affected while the phages remain intact. Another possibility is that some intracellular protein binds to the pIII coat proteins or to the QPSPSPT sequence itself. This could explain the proportion of labeled phages detected in the cytoplasm and relatively far from the nuclei of the cells. This should be tested experimentally, and there are multiple ways to do so. One way would be to perform a time-course fluorescence microscopy experiment focusing on a single cell or group of cells in the presence of labeled phages. This would theoretically show phage-cell interaction, including the lifetime of the labeled phage once inside a eukaryotic cell.

Fluorescence imaging of the intracellular localization of an M13 bacteriophage displaying the heptamer peptide on its pIII coat protein was an important verification step in the process of isolating and characterizing a novel nuclear localization sequence.

Fluorescence microscopy and subsequent imaging processing provided a precise method of localizing phage position in the cell. By labeling the phage coat protein pVIII directly with an amine-reactive fluorochrome, the complications and uncertainties of immunohistochemistry were avoided. Because fluorochrome-labeled phage retains at least some of its function[39], time-lapse studies can be performed more easily and with better controls than a typical study that requires immunohistochemistry. Direct fluorochrome labeling of phage also incurs a substantial reduction in materials cost in comparison to immunohistochemistry. The wide range of excitation and emission wavelengths for amine-reactive fluorochromes allows for many interesting color combinations and applications.

While nuclear localization of QPSPSPT-bearing phage was observed, the variability in measured outcomes could use improvement. In order for the isolated peptide to be ideal for gene therapy, it would need to confer the ability to transfect the great majority of malignant cells. Furthermore, improved consistency of nuclear localization would require a lower dose of whatever therapy is associated with the peptide, thereby reducing cost, toxicity, and side effects.

Fluorochrome-labeling may reduce the ability of phage to penetrate eukaryotic cells and localize to the nucleus. The amine-based reactive chemistry used to conjugate Alexa Fluor to the phage has nominally equal affinity for all coat proteins, including the five copies of pIII that display the targeting peptide. An increase in phage diameter or interference with the five pIII coat proteins displaying the nuclear localization sequence are two ways in which nuclear targeting could be diminished. There are approximately 2,700 copies of the pVIII coat protein on the surface of an M13 phage. The ratio of pIII

to pVIII (5:2700) was leveraged with careful selection of the Alexa Fluor concentration to minimize fluorescent labeling of the displayed peptide in order to preserve targeting function. The likelihood of many phages having the heptamer peptide fouled by the fluorescent label is therefore infinitesimal. However, the addition of multiple fluorochromes onto the phages could increase its hydrodynamic radius, making active transport of the phages into eukaryotic cells more difficult.

An important practical assessment of the QPSPSPT peptide's ability to localize to cell nuclei would involve its incorporation into a non-viral gene therapy construct such as a liposome. Incorporation of polylysine into cationic liposomes has shown to improve their efficacy by an order of magnitude[7]. Incorporation of the nuclear localization sequence from the large T antigen of the SV40 virus has been shown to increase transfection by one to three orders of magnitude[42]. Bacteriophages do not normally enter eukaryotic cells or localize to eukaryotic nuclei, and this inherent characteristic may confer a disadvantage to the nuclear targeting ability of the QPSPSPT peptide. Bacteriophage display is an effective method for isolating novel peptides. However, their use in gene therapy is minimized by their lack of affinity for eukaryotic cells and their ability to cause inflammation. The QPSPSPT peptide should be tested in non-viral gene therapy constructs to evaluate its clinical potential.

The interaction of the QPSPSPT peptide with nuclear structures could be studied further by incorporating the peptide into alternative reporters such as nonviral gene therapy constructs or by ligating the peptide to radioactive or fluorescent markers such as quantum dots. The discovery of future peptides relevant to flexible and therapeutic

approaches will likely still rely on biopanning experiments similar to those described by Ashley Aston-Weiner and visual confirmation experiments as described here.

CHAPTER III

MANUSCRIPT 2: DETECTION OF MATRILYSIN BY FIVE CANCER CELL LINES

Introduction

Matrix metalloproteinases

Matrix metalloproteinases (MMPs) are a group of 23 enzymes produced by human cells. Their name implies two characteristics. First, this class of proteins is collectively able to break down every known and tested component of the extracellular matrix. Second, these enzymes are regulated by, and are dependent upon, a zinc ion[90]. There is an unpaired cysteine, Cys[73], in the cleavable pro-domain of the zymogen form of MMPs that binds to a zinc atom. As long as the pro-domain is in place, the zymogen is inactive and hydrophobic. A change in conformation or proteolysis (either from autolysis or other proteinases) results in detachment of the thiol group of the cysteine (known as a "cysteine switch") from the zinc ion allowing water to hydrolyze the zinc ion, and activating the MMP[80].

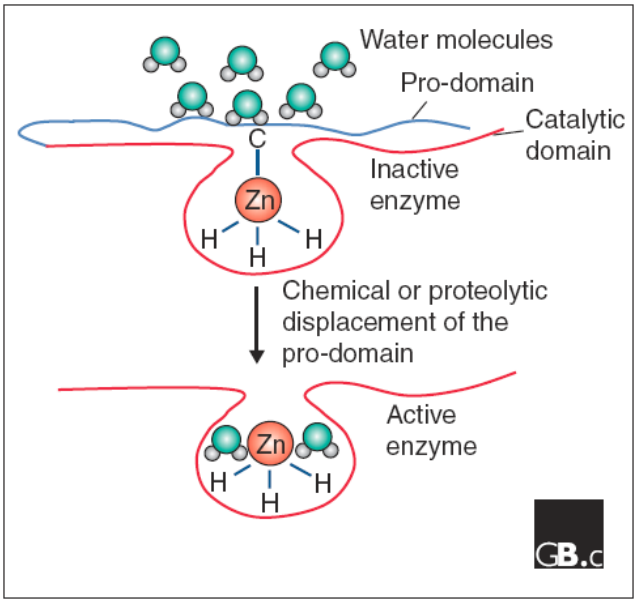

Figure 9: Matrix metalloproteinases are activated by cleavage of the pro-domain, which also makes the enzyme water soluble[75].

MMPs are typically subdivided into six groups. The first four groups are named after their primary substrate, but most MMPs within these groups have other substrates as well. The collagenases include MMPs 1, 8, and 13. The gelatinases include MMPs 2 and 9. The stromelysins include MMPs 3, 10, and 11. The matrilysins include MMPs 7 and 26. The membrane-type MMPs constitute the fifth group, and as the name suggests, they are bound to the cell surface. MMPs 14, 15, 16, 17, 24, and 25 are in this group, and their primary substrates are gelatin, fibronectin, and laminin. The sixth group contains the rest of the MMPs: 12, 19, 20, 21, 23, 27, 28. The substrates of this last group of metalloproteinases are either not known or not easily categorized[75].

In healthy humans, the MMPs are highly regulated and serve a variety of tissue remodeling functions such as wound healing[71], angiogenesis[25], involution of the prostate after castration[89], bone and tooth growth and remodeling[90], immune defense[9,87], reproductive function[15], or vascular permeation to allow the passage of immune system cells like macrophages[16]. The MMPs are regulated at every step from transcription to zymogen activation. The MMPs are essential for life, as evidenced by the early death of knockout mice lacking genes for MMPs. However, the degradation capabilities of the MMPs also aid migrating cancer cells during metastasis[72]. Thus, MMPs have gained status as prognostic indicators of metastasis and as drug targets. MMPs have a wide variety of substrates, and can be both helpful and harmful to healthy tissue[3,13]. Their propensity to either end takes into account many factors and is therefore not easily defined.

MMPs become a problem when they are not properly physiologically regulated[10]. Along with cancer, abnormalities in MMP regulation can become a factor in various

cardiovascular ailments such as myocardial infarction and atherosclerosis, as well as in inflammatory disorders such as rheumatoid and osteoarthritis. Once MMP balance is disrupted, the destructive momentum can increase rapidly[6]. MMPs can cleave other MMPs, thereby increasing the varieties of ECM substrates vulnerable to cleavage. Cleavage of the ECM can reveal hidden domains in the matrix proteins that serve as growth or migration-promoting factors. Furthermore, cleavage of cell-surface proteins such as E-cadherin, FGF, TGF-β, IGF, TNFα, Fas ligand, and IL-1β can promote cell migration and invasion, or prevent the cell from receiving apoptosis signals[80].

Several MMP inhibitors, both specific and broad spectrum, have reached clinical trials[85,84,66,23]. These trials as a whole were unsuccessful; one MMP inhibitor, tanomastat, was found to accelerate the progression of the cancer. The most common problem with these drugs was musculoskeletal side effects. Based on preclinical evidence, however, it could be argued that these trials were not thorough enough to sufficiently evaluate the potential of MMP inhibitors. The trials were based on the "brute force" approach of the maximum tolerated dose rather than using escalating dosage patterns. Furthermore, the trials focused on patients in the later stages of cancer. Another reason for the ineffectiveness of these treatments could be surmised from the results of studies in knockout mice that show upregulation of other MMP species to compensate for a reduction or loss of function of one or a few members of the family[90].

Matrilysin

MMP-7, hereby referred to as **matrilysin**, is the smallest of the known metalloproteinases, along with MMP-26[24]. It contains only the domains necessary for

secretion and function: a signal peptide, a cleavable pro domain, and a catalytic domain, achieving a molecular weight of approximately 28 kDa in its passive form and 19 kDa in its active form (sans pro domain). It lacks a hinge region, as well as fibronectin repeats and hemopexin-like domains found in other MMPs. Its diminutive structure does not limit its range of function, as it is a valuable enzyme to healthy and malignant tissue alike[33]. So far, matrilysin is known to assist in healthy body function by maintaining immune function[73], wound healing, and degradation of non-essential or exhausted tissue (especially during embryonic development). It is constitutively expressed by a variety of exocrine glands, including mammary glands, the liver, the prostate, the pancreas, intestinal tissue[45], and the peribronchial glands. Matrilysin also plays a crucial role in tumor progression, allowing degradation of ECM components and activation of hormones and growth factors, both of which assist tumor proliferation and migration, up to and including metastasis[14].

Matrilysin's methods of assistance to healthy and malignant tissue extend beyond the sole function of extracellular matrix degradation. Injured lung epithelial cells secrete matrilysin at their basal surface. In this case, matrilysin cleaves syndecan-1, which binds to a chemokine[44]. This creates a chemokine gradient that orients migrating neutrophils. Matrilysin is expressed at injury sites in the lung epithelium, and although the reason is unknown, matrilysin is necessary for normal wound healing. Knockout mice lacking the matrilysin gene have severe lung wound repair defects; these defects are worse than defects caused by the knockout of other MMP genes.

Matrilysin has been shown to aid in immune function in several ways. One famous way involves the activation of α-defensins in mice, also known as cryptdins --

small antibacterial peptides. Matrilysin cleaves the precursor form of the cryptdin, activating it and allowing the peptide to puncture bacterial membranes. In normal mice, matrilysin expression parallels cryptdin expression. In knockout mice lacking the gene for matrilysin, no cleavage of the procryptdin occurs and the ability to battle enteric pathogens is substantially inhibited[9]. Matrilysin also assists with macrophage invasion. Macrophages produce matrilysin, which helps them degrade and extravasate through the extracellular matrix. Another study shows that matrilysin is required for herniated disc resorption by macrophages. In this scenario, the presence of matrilysin was also required for the secretion of TNF-α, an inflammatory mediator[31].

However, matrilysin is also of tremendous help to growing and metastasizing tumors, as evidenced by its expression in tumors of every organ type. In fact, the presence of matrilysin mRNA is shown to increase with the stage of cancer and during dysplasia and metastasis[47]. When it comes to cancer, an increase in matrilysin worsens the prognosis[41]. While many studies focus on the negative influence of matrilysin on cancer survival, there is also new evidence of a correlation between the presence of matrilysin and favorable prognostic markers.

Matrilysin is known to be important in regulating cell-surface proteolysis. It can bind E-cadherin, β-catenin, Fas ligand, TNF-α, and heparin sulfate[47,59]. A recent paper by Nakamura et al details the cleavage of the entire six-variant spectrum of Insulin-like Growth Factor Binding Proteins (IGFBP) by matrilysin. IGFBP is a modulator of Insulin-like Growth Factor (IGF) availability, and thus this action liberates IGF, which can then help a growing tumor acclimate to its surroundings[60].

Another negative role of matrilysin is its involvement in atherosclerosis in humans. Matrilysin, along with several other MMPs, is secreted by lipid-laden macrophages buried behind the fibrotic tissue of a vessel wall lesion. The finding that matrilysin has two major substrates in an atherosclerotic lesion, versican and tissue factor protease inhibitor, suggests the role of matrilysin in both plaque destabilization and downstream thrombosis formation[62].

Clinical trials involving inhibitors of matrilysin have proven unsuccessful. However, much has been learned about these enzymes in the course of developing inhibitors for them. Cleavage sequences for some MMPs are now known, and they will likely prove valuable for the newest class of targeted nanoscale imaging and therapeutic solutions. These constructs involve the use of fluorescent functionalized nanoparticles such as quantum dots and an attached peptide linker which can be proteolytically cleaved to allow drug interaction or fluorescence.

To date, no published study has attempted to quantify the amount of matrilysin produced by cancer cells using proteomic analysis. mRNA analysis has been attempted using RT-PCR, but this is an indirect, non-quantitative measure of actual protein production, as the mRNA transcripts can be degraded before translation. Furthermore, a single mRNA can be translated multiple times before it is degraded. A more accurate way to measure matrilysin would be the through the use of an ELISA using antibodies specific for matrilysin, which measures the amount of protein present, or by using an activity assay, from which the concentration of matrilysin in a supernatant sample could be calculated.

Cathepsin D

Cathepsin D is an aspartic protease that is overexpressed and hypersecreted by epithelial breast cancer cells[28]. Like matrilysin, elevated levels of cathepsin D are associated with poor prognosis, as the enzyme is known to stimulate tumorigenicity and metastasis. Cathepsin D modified by mutation to be enzymatically inactive can still function as a mitogen. This suggests that cells possess a receptor specific for cathepsin D, although one has yet to be located. Other paracrine actions of cathepsin D are the stimulation of angiogenesis, remodeling of the extracellular matrix, decreased apoptosis, and increased motility. There is also evidence that cathepsin D in its zymogen form serves as a promoter of fibroblast outgrowth[56]. Cathepsin D has no known endogenous inhibitor, but expression is thought to be highly regulated by estrogen[28].

Cancer cell lines

MCF-7 cells are a well-known and well-characterized epithelial breast cancer cell line[82]. In normal culture, they produce small amounts of matrilysin[82]. However, MCF-7 cells have also been shown to increase their production of matrilysin when exposed to certain hormones in culture such as relaxin and epidermal growth factor[14]. This is important because in a physiological setting, oncogenic upregulation of particular factors could change the production level of matrilysin.

MCF10A is an immortalized, non-tumorigenic cell line isolated from benign breast fibromas. Like normal breast cells, the MCF10A cell line forms three dimensional, dome-like acinar structures in collagen, its growth can be controlled by exogenous growth factors, and adhesion is required in order to proliferate[76].

SW480 and SW620 cells are isolated from malignant epithelial colon tumors. SW480 cells are not known to produce matrilysin in culture. SW480NEO cells possess an insert that confers resistance to neomycin. SW480MAT cells possess the ampicillin resistance insert but also possess an insert for enhanced production of matrilysin. SW620 cells have shown the ability to produce matrilysin in culture[95].

Materials and Methods

Western blotting – sample preparation

Cultures of SW480NEO, SW480MAT, and SW620 colon cancer cell lines were obtained from Oliver McIntyre (Vanderbilt University, Department of Cancer Biology). Vials of frozen MCF10A and MCF-7 were obtained from American Type Culture Collection (CRL10317 and HTB-22, respectively). All cell lines were grown in T-75 flasks to 70% confluency. At this point the supernatant was removed and replaced with serum free media. After 48 hours the supernatant from each flask was removed and centrifuged through an Amicon Ultra 10 kDa molecular weight cutoff filter (Millipore, UFC900508) and the residual fluid was recovered. Recombinant human matrilysin and MMP-13 obtained from R & D Systems (WBC016, WBC030, respectively) as well as concentrated matrilysin provided by Dr. Michael van Saun of the Lynn Matrisian lab (Vanderbilt University, Department of Cancer Biology) were used as positive controls. DMEM with 10% FBS (Atlanta Biologicals, S11150) was used as a negative control.

Western blotting – gel electrophoresis

The samples were then loaded into a 10% Tris-Tricine gel (Life Therapeutics, NT11-010), and the gels were electrophoresed at 150 V for one hour in a Bio-Rad Mini-Protean II electrophoresis chamber (165-2960). A coomassie blue assay was performed in a separate electrophoresis run to verify correct technique before attempting the Western blot. Electrophoresed gels were blotted to an Immobilon-P^{SQ} PVDF membrane (Millipore, ISEQ10100) designed to more efficiently retain small proteins. Total protein

stain on the blot was performed using SYPRO Ruby fluorescent stain (Molecular Probes, S-12001) to verify successful blotting. Blocking of the membrane was performed with 2.5% Carnation Dry Milk and 0.05% TWEEN-20 (Sigma, P-5927) in standard Tris Buffered Saline (TBS) (Sigma, T3203). After three 15 minute washings in TBS, primary antibody incubation was performed at a dilution of $1:10^4$ overnight on a platform shaker at 4° C. After three 15 minute washings in TBS, the blot was incubated with secondary fluorescent-conjugated antibody at a dilution of $1:10^4$ for one hour at room temperature.

Western blotting - detection

The imaging strategy involved the use of secondary anti-mouse antibodies (Molecular Probes, A-21093) conjugated to Alexa Fluor 350 fluorophores to bind to the primary antibodies (Murine anti-MMP-13 and anti MMP-7, EMD Biosciences, IM71T and IM78T) on the blot. Blots were then imaged in a BioDocIt gel box (UVP, Cambridge, MA). To verify feasibility, 5 μL of secondary antibody suspension was pipetted onto a small piece of blotting membrane, and the membrane was placed in the gel box with the UV light source set to 350 nm. The antibody suspension exhibited strong fluorescence and was easily imaged by the gel box camera.

Immunoprecipitation

Immunoprecipitations were performed using the Sigma Protein G Immunoprecipitation Kit (IP-40, Sigma, Inc.). 200 μL of supernatant from each of the cell culture samples incubated in serum-free medium were transferred to the included microcentrifuge spin columns. 2.5 μg of purified monoclonal antibodies to the protein of

interest (matrilysin or cathepsin D) were also added to the spin columns, along with 400 μL of the included immunoprecipitation buffer. The spin columns were capped and placed on a rotisserie mixer for at least 4 hours at 4º C. In the meantime, 30 μL per spin column of the protein G agarose beads included in the kit were washed twice with 1 mL of cold immunoprecipitation buffer and resuspended in 50 μL of immunoprecipitation buffer. After the incubation, the washed protein G beads were transferred to the spin columns, and the columns were incubated at 4º C for at least 4 hours on a rotisserie mixer.

After the incubation, the columns were centrifuged to remove unbound protein and antibodies. The spin columns were then washed by adding immunoprecipitation buffer and centrifuging five times. One additional wash was then performed with low-strength (0.1X) immunoprecipitation buffer. 40 μL of Tris-Tricine-SDS Sample Buffer (Gradipore, BG-125) were added to each of the columns, and the columns were immersed in boiling water for five minutes. The spin columns were then centrifuged to collect eluted proteins, and the effluent from each column was loaded onto a 10% Tris-Tricine gel. The gel was electrophoresed at 150 V for one hour, and the gels were stained with coomassie blue (ICN, 190343) overnight and destained with a solution of 10% methanol (Fisher Scientific, TIA947-4) and 7% acetic acid (Fisher Scientific, A35-500) until an acceptable amount of the coomassie stain was removed.

MMP assay – cell kinetics measurement

Cell lines were maintained in T-75 flasks (Falcon, 353136) under standard culture conditions. MCF-7 and MCF10A lines had specific media formulations, while the sw480

and SW620 colon carcinoma lines used a common media (see Appendix A). Eight six well plates, one for each time point, were seeded with approximately 10^5 cells per well based on a cells/mL count obtained from a Beckman-Coulter Multisizer 3 particle counter. Each cell line occupied one well in each of the six-well plates, and appropriate growth media was added up to 2 mL per well. At each time point, 200 µL of supernatant from each well were placed in microfuge tubes and stored at -70° C. The rest of the media was aspirated from each well and replaced with 1 mL of 1X Trypsin-EDTA solution (Gibco 25200-056). Cells/mL counts were then obtained using a Beckman-Coulter Multisizer 3 Particle Counter.

MMP activity assay

A fluorescence-based enzymatic activity assay (Enzolyte 520 Assay kits, Anaspec, 71150 and 71153) was performed to determine the presence and concentration of matrilysin. 50 µL of cleavable substrate specific for matrilysin were added to each well of a 96 well plate (Sigma, N1142), and 50 µL of supernatant mixed with 1 mM APMA (included in the kit) were put into the appropriate well. The plate was incubated for 30 minutes at room temperature before the fluorescence readings were recorded. The MCF-7, SW480MAT,

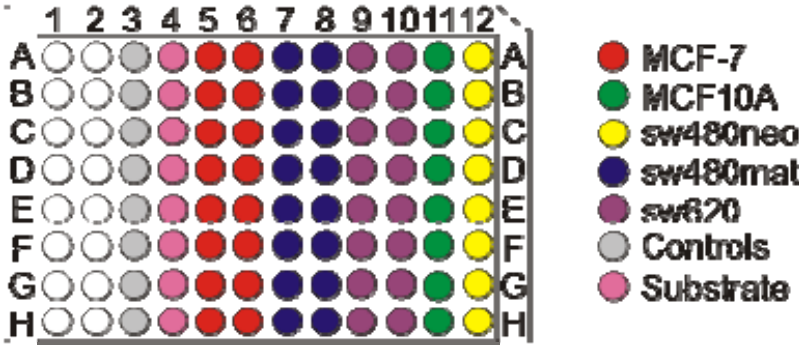

Figure 10: Fluorescent substrate assays were performed on a 96-well plate according to the setup shown.

and SW620 cell lines had two sets of columns, while SW480NEO and MCF10A only had one column apiece due to substrate limitations (Figure 10). Controls included assay buffer only, water only, and media only. All assays mentioned in this paper were performed in black 96-well plates (Sigma CLS3991) using a Bio-Tek Synergy HT Plate Reader.

MMP assay – antibody-based ELISA

An ELISA based on antibodies to the zymogen form of MMP-7 (Amersham Biosciences, RPN2620) was performed using the supernatants from MCF-7 and MCF10A cell lines. Standard wells were set up on the same plate in parallel with the sample wells according to the kit instructions. 100 μL of cell culture supernatant were pipetted into the appropriate wells, 10 μL of 20mM EDTA were added to each well, and the plate was incubated in the dark at 4° C for 16 hours. All wells were then washed with the wash buffer included in the kit. After washing, 100 μL of peroxidase conjugate were pipetted into each well and the plate was incubated in the dark at 4° C for 1 hour. All wells were then washed four times with wash buffer and 100 μL of TMB substrate were immediately added to each well. The plate was then stored at room temperature in the dark for 30 minutes. 100 μL of 1 M sulfuric acid were then added to all wells to stop the reaction. The plate was read in a Bio-Tek Synergy HT Plate Reader at 450 nm.

Substrate tests

The same substrate used in the Enzolyte MMP-7 assay kit was purchased separately from Anaspec (catalog #60574-01). Substrate arrived desiccated in 0.1 mg

aliquots. When ready for use, the substrate was solubilized in 60 µL of dimethyl sulfoxide (DMSO). Solubilized substrate was further diluted 1:100 with assay buffer provided in the Enzolyte kit. Substrates were incubated with cell culture supernatant, with some samples supplemented with 10 µL of Roche Complete Protease Inhibitor (mini tablets dissolved according to manufacturer's instructions) (Roche, 11836170001) and/or 10 µL of 0.2 M EDTA (Fisher, C-3920), pH 9.0.

Results

Western blot detection of matrilysin synthesis

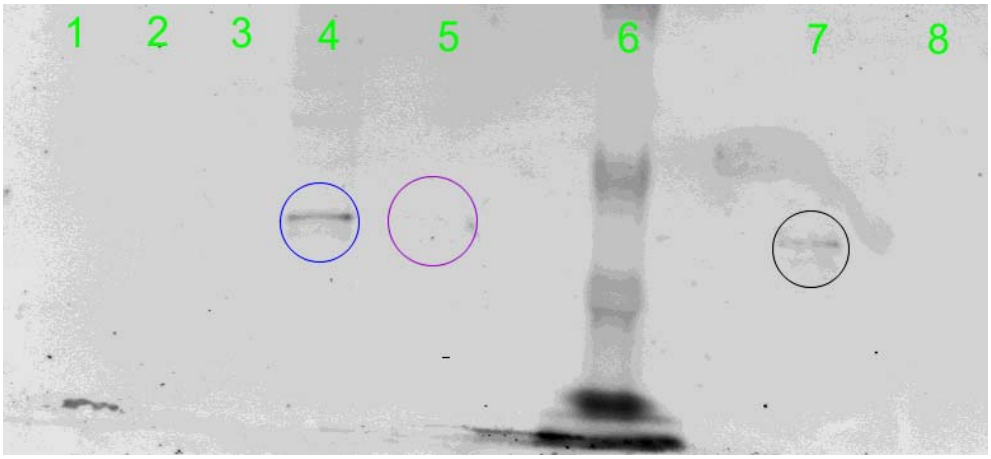

Figure 11: Western blot using infrared-absorbing secondary antibodies. Blue circle denotes signal from SW480MAT lane, violet circle denotes faint SW620 signal, black circle denotes positive control. Lanes from left to right: 1--MCF-7, 2--MCF10A, 3--SW480NEO, 4--SW480MAT, 5--SW620, 6--ladder, 7--MMP-7enzyme control, 8--MMP-13 enzyme control.

A Western blot for matrilysin production produced a positive result for SW480MAT cells and a possible positive result for SW620 cells. The band corresponding to SW620 was not as pronounced as the SW480MAT and control bands. (Figure 11). No bands consistent with matrilysin production were detected under the same conditions for MCF-7, MCF10A, or SW480NEO.

Fluorogenic substrate detection of matrilysin synthesis

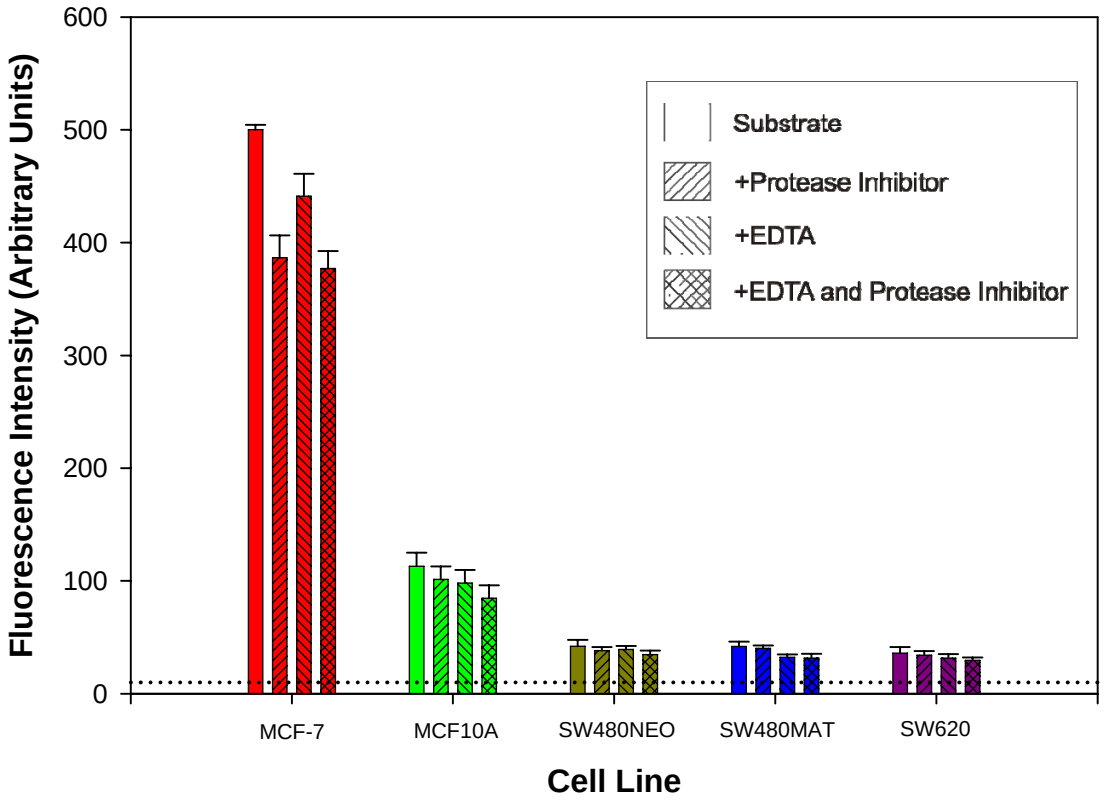

Figure 12: Matrilysin synthesis assessed by cleavage of a specific fluorogenic assay. Fluorescence readings vary, but only slightly, based on the addition of protease inhibitor and EDTA. Supernatant for MCF-7 cell culture was most effective in fluorogenic substrate cleavage. Cell supernatants with positive Western blot results have the weakest capacity for substrate cleavage. The dotted line represents average background fluorescence. MCF-7, MCF10A, and SW480MAT cell line statistics for uninhibited substrate cleavage are based on 4 repeats. SW620 and SW480NEO cell line statistics for uninhibited substrate cleavage are based on 2 repeats. Protease inhibitor and EDTA statistics for all cell lines are based on 3 repeats.

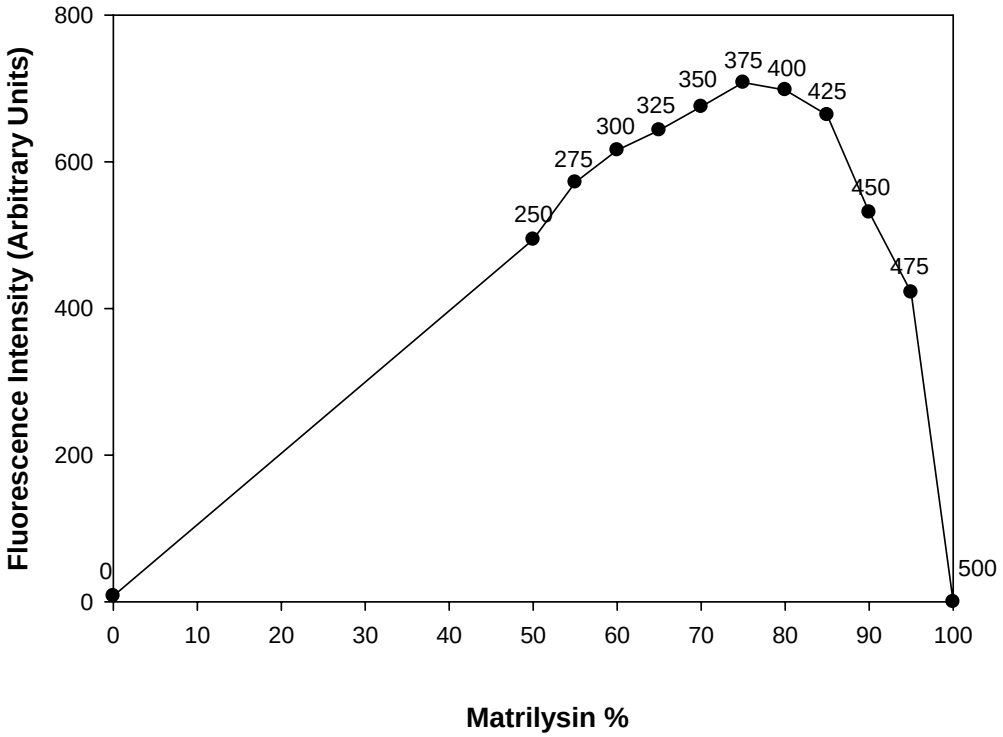

Figure 13: Matrilysin substrate cleavage by purified, active-form matrilysin. The numbers above the data points indicate concentration of matrilysin, in nanomolar units. Only one set of data was obtained in order to verify enzyme and substrate function.

Fluorogenic substrate cleavage was not consistent with the Western blot results. Supernatants from MCF-7 cells produced significantly greater cleavage of the fluorogenic substrate than the SW40MAT and SW620 cell supernatants, which were detected as positive for matrilysin by Western blot (Figures 11, 12). Supernatant from cells in culture for 48 hours was added to the substrate. Substrate cleavage is slightly reduced by addition of broad-spectrum protease inhibitor and EDTA to inhibit metalloproteinases. However, neither of the inhibitors, alone or together, can fully inhibit non-specific substrate cleavage. EDTA inhibited cleavage of the substrate by purified matrilysin, as indicated by a reading of 14 +/- 1 units, a reading only slightly above the background fluorescence level of 8 +/- 2 units (Figure12).

A one-way ANOVA was performed on the data to determine if a significant difference was present amongst the fluorescence intensity measurements. Analysis of measurements from wells without protease inhibitors gave a P value of less than .001, indicating a significant difference amongst the fluorescence intensity readings for each cell line. ANOVA analysis was also performed to determine if differences were significant amongst the fluorescence intensity readings for the inhibited and uninhibited substrate cleavage for each cell line. The results indicated that significant differences in cleavage were present amongst the readings for MCF-7 (P = 0.003), but not MCF10A, SW480NEO, SW480MAT, or SW620.

Fluorogenic substrate detection of MMP-13 synthesis

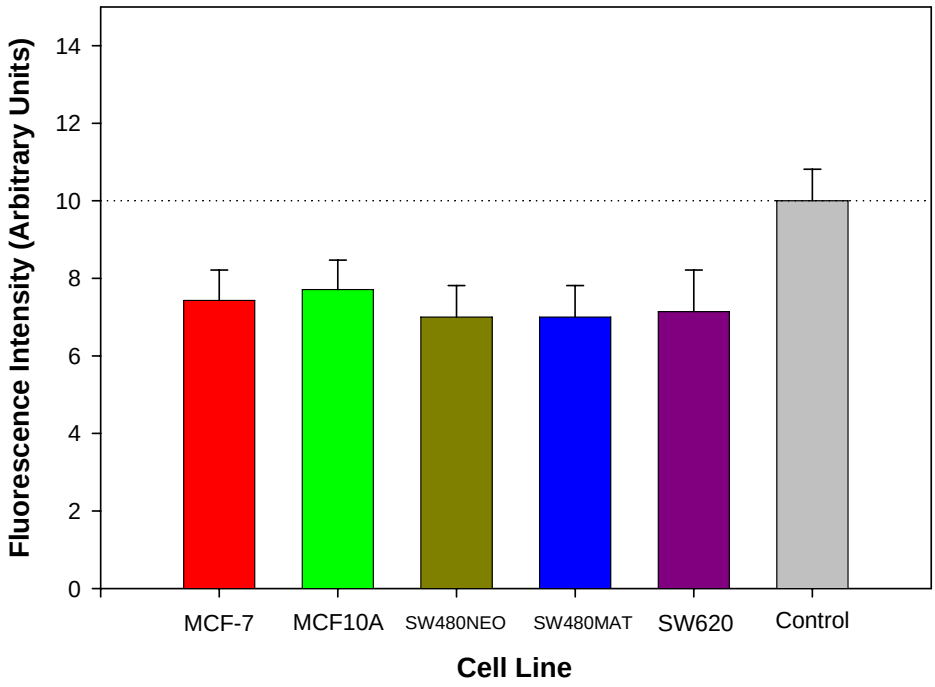

Figure 14: Results of an assay for MMP-13 in the supernatants of five cell lines. The supernatants failed to cleave a fluorogenic substrate specific for MMP-13. Substrate in assay buffer with no supernatant added is shown as the control. Bar height is mean plus standard deviation. n=8 for each cell line.

Figure 14 shows that none of the cell supernatants gave fluorescence readings above the background level of 10. Therefore, the data indicate that none of the cell lines produced detectable levels of MMP-13. Water, assay buffer, and empty wells all gave readings of zero. 250 nM MMP-13 enzyme added to the substrate as a positive control gave readings of 213 +/- 5 units. A one-way ANOVA test was performed to test for a statistically significant difference amongst the data. The test returned a P value of 0.468, indicating that no significant difference was present.

Immunoprecipitation detection of cathepsin D

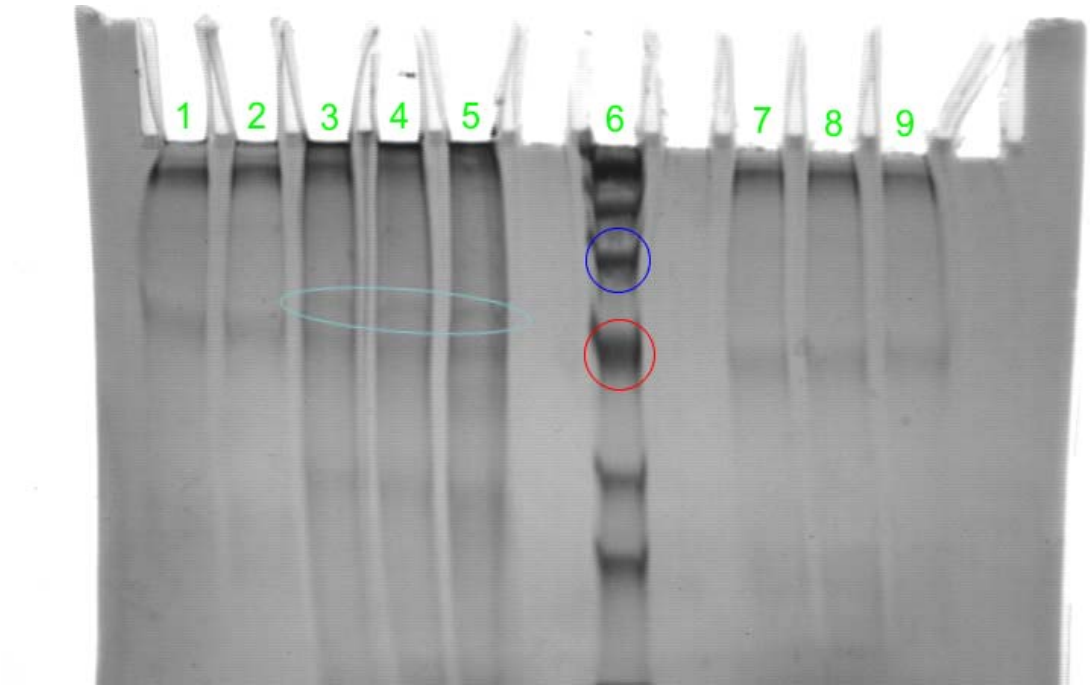

Figure 15: Immunoprecipitation performed on supernatants of seven cell lines gives light bands corresponding to the predicted molecular weight of reduced cathepsin D in three of the lanes (aqua oval). The lanes are numbered as follows: 1 – MCF-7, 2 – MCF10A, 3 – SW480MAT, 4 – SW480NEO, 5 – SW620, 6 – molecular weight ladder, 7 – corneal epithelial cells, 8- dermal fibroblasts, 9 – cell culture media only. The red circle denotes the ladder band corresponding to 56 KDa; the blue circle denotes the ladder band corresponding to 101 KDa. Expected molecular weight of reduced cathepsin D is ~65KDa. The image is representative of four repeats.

Immunoprecipitation performed on supernatants from the five cancer cell lines as well as supernatants from corneal epithelial cells (ATCC Catalog #CRL-11135) and dermal fibroblasts (ATCC Catalog #CRL-1554) kindly provided by the Rick Haselton lab (Vanderbilt University, Department of Biomedical Engineering) revealed faint bands corresponding to the predicted molecular weight of reduced cathepsin D in the lanes corresponding to SW480MAT, SW480NEO, and SW620. Bands appeared in every lane in a region approximately in line with the 56 KDa marker, and were likely antibody fragments (Figure 15).

ELISA detection of matrilysin synthesis as a function of time in culture

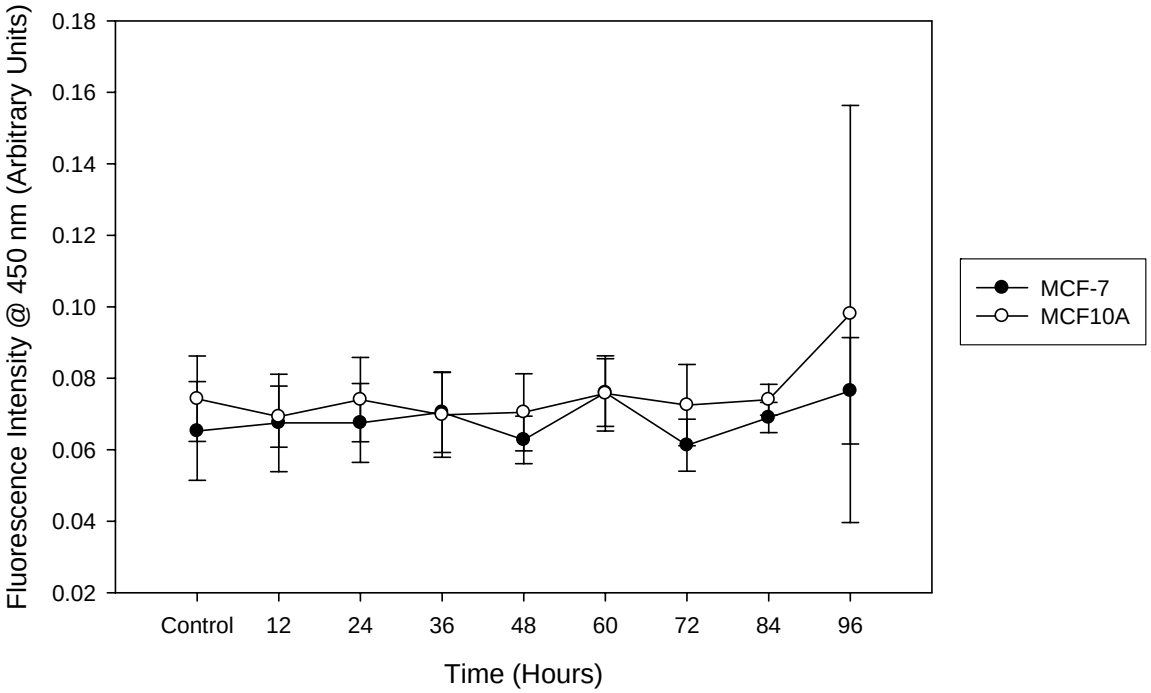

Figure 16: ELISA for detection of matrilysin zymogen by MCF-7 and MCF10A cell lines is consistently negative over a 96-hour interval. Data points indicate mean + standard deviation. n=2

None of the time points in Figure 16 gives a signal significantly stronger than that of the control. The detection threshold of the assay corresponded to a signal intensity of 0.07 ± 0.01, equivalent to a concentration of 5.07 pM or (97 pg/mL, given in the accompanying product literature). A one-way ANOVA was performed on the data to determine if the signals from either cell line were significantly different from that of the control signals. For MCF-7, the P value was 0.848, and for MCF10A the P value was 0.711. Both values indicate that no significant difference was present in the data.

Discussion

Table 2: Summary of proteolytic enzyme synthesis results as a function of cell line and detection approach obtained using the detection methods employed in this study. +++,++, and + indicate strong, moderate, and weak positive results, respectively. – denotes a negative result. "nd" indicates that results were not obtained.

	MCF-7	MCF10A	SW480NEO	SW480MAT	SW620
Western blot: MMP-7	-	-	-	+++	+
Activity assay: MMP-7	+++	++	+	+	+
Activity assay: MMP-7 + protease inhibitor	+++	+	+/-	+/-	+
Activity assay: MMP-7 + protease inhibitor + EDTA	+++	+	+/-	+/-	+
ELISA: MMP-7	-	-	nd	nd	nd
Western blot: MMP-13	-	-	-	-	-
Activity assay: MMP-13	-	-	-	-	-

Western blotting confirmed the presence of matrilysin in SW480MAT and SW620 cell cultures, in agreement with other studies[95]. Western blotting did not detect matrilysin production by MCF-7, MCF10A, or SW480neo cell lines. However, a fluorogenic assay was performed to confirm the Western blots and to estimate the production rate of matrilysin by the cell lines over a 96-hour time course. The commercially availably intensity assay uses a fluorogenic substrate uniquely cleavable by matrilysin, although some cross-reactivity with MMP-13 is reported by the manufacturer. Fluorescence intensity is proportional to the amount of matrilysin activity in the sample, enabling a quantitative result.

A similar commercial assay, specific for MMP-13, was used to assess the potential for matrilysin substrate cleavage by the presence of MMP-13. None of the cell lines produced detectable levels of MMP-13 (Figure 14) and MMP-13 was presumed to be absent in the fluorogenic substrate assessment.

The results of the fluorogenic matrilysin assay were not consistent with the Western blot results in this study or the other reports in the literature. Matrilysin synthesis by SW480MAT and SW620 cells detected by Western blotting was not confirmed by cleavage of the matrilysin-specific fluorogenic substrate. Of equal significance was the matrilysin substrate cleavage observed in MCF-7 (and, to a lesser extent MCF10A and SW480NEO) cells without confirmation by Western blotting or literature reports. Fluorescent substrate cleavage by a non-matrilysin, non-MMP-13 enzyme is one hypothesis consistent with the observed results.

Experiments designed to test this hypothesis were conducted with cell culture supernatants supplemented with broad-spectrum protease inhibitors and/or EDTA, a metalloproteinase inhibitor. The results of these experiments were consistent with cleavage of the matrilysin assay substrate by a mechanism other than matrilysin or other MMPs. Fluorescent signal in the presence of strong, multifunctional protease inhibitors is consistent with substrate cleavage by mechanisms other than matrilysin or other metalloproteinases (Figure 12). The use of this fluorogenic substrate or a matrilysin detection method in complex systems such as cell culture supernatants must be approached with caution.

Chelation of divalent cations by EDTA supplementation, a necessary cofactor for MMP activity, did not significantly reduce substrate cleavage mediated by cell culture supernatants. Combined with undetectable substrate cleavage induced by cell culture medium alone, this result suggests that a cell-derived product other than a divalent cation-sensitive protease is capable of cleaving this substrate.

The addition of a protease inhibitor mixture failed to prevent substrate cleavage by cell culture supernatants. Since this result alone could not exclude MMP activity as responsible for substrate cleavage, a set of experiments was conducted using cell culture supernatants supplemented with both EDTA and protease inhibitor. This broad inhibition strategy retained the capacity for fluorogenic substrate cleavage. Tests with culture supernatant, protease inhibitor, and the fluorogenic substrate indicated that cleavage of the substrate by cell supernatants was only slightly reduced in the presence of protease inhibitor, and the results were all above the background readings for every cell line (Figure 12).

The commercially obtained protease inhibitor is not effective against aspartic proteases or metalloproteinases. The potential for a cell-derived aspartic protease to be present in the supernatant, uninhibited by EDTA plus the commercial protease inhibitor product, and capable of fluorogenic substrate cleavage remained a candidate hypothesis consistent with the experimental results. Cathepsin D is an aspartic protease that is known to be upregulated in some cancers. However, immunoprecipitation using antibodies to cathepsin D and concentrated supernatant samples from the five cell lines failed to reliably detect cathepsin D (Figure 16). The mechanism of nonspecific substrate cleavage remains unknown.

Future work could be performed to determine what is causing nonspecific cleavage of the matrilysin substrate, but these data indicate that quantitative determination of matrilysin by a fluorogenic substrate in complex cell culture supernatant is not currently possible. Future work with the cell lines could study the kinetics of their progression through an artificial matrix such as Matrigel in comparison to cell lines not

isolated from tumors. Selective addition of active proteases known to be produced by MCF-7 and MCF10A cell lines to non-migrating cell lines in the presence of Matrigel could also help to identify the proteases specifically responsible for cleavage of substrate motifs mimicking those present in extracellular matrix. Protease inhibitors have been studied as possible anticancer therapeutic agents. Furthermore, precise knowledge of upregulated proteases could lead to more specific and possibly more effective inhibitors of cancer cell migration.

APPENDIX A: Cell Media Recipes

MCF-7 media

50 ml FBS
5 ml Non-essential amino acids (purchased as a solution)
5 ml sodium pyruvate (purchased as a solution)
0.5 ml insulin (purchased as a solution)
5 ml antibiotic-antimycotic
435 ml MEM

MCF10A media

25 ml FBS
10 µl EGF (this is reconstituted at the suggested concentration)
50 µl cholera toxin (this is reconstituted at the suggested concentration)
0.5 ml insulin (purchased as a solution)
1.4 ml hydrocortisone (purchased as a solution)
5 ml antibiotic-antimycotic
468 ml DMEM-F12

Sw620 media

50 mL FBS
450 mL DMEM (high glucose, L-glutamine, with pyridoxine HCl, without sodium pyruvate)

Sw480neo/mat media

Same as SW620 except add 5 mL of neomycin and remove 5 mL of DMEM

Ordering Information:

Calbiochem:
Cholera Toxin - 227036

Invitrogen:
MEM - 11095-080
DMEM/F12 - 11330-032
Antibiotic-antimycotic - 15240-062
EGF – 13247051

Sigma:
Insulin Solution - I0516
Hydrocortisone - H6909
Sodium Pyruvate Solution (100 ml) - S8636
MEM Non-essential Amino Acid Solution (100 ml) - M7145

Atlanta Biologicals:
Defined Fetal Bovine Serum – S11150

APPENDIX B: Phage DNA Sequence

NNNNNNNGNCGNNTTCNGACGTTAGTAATGAATTTTCTGTATGGGATTTTGCTAAACAACTTTCAACAGTTT
CGGCCGAACCTCCACCCGTAGGAGAAGGCGAAGGCTGAGAGTGAGAATAGAAAGGTACCACTAAAGGAATTG
CGAATAATAATTTTTTCACGTTGAAAATCTCCAAAAAAAAGGCTCCAAAAGGAGCCTTTAATTGTATCGGTT
TATCAGCTTGCTTTCGAGGTGAATTTCTTAAACAGCTTGATACCGATAGTTGCGCCGACAATGACAACAACC
ATCGCCCACGCATAACCGATATATTCGGTCGCTGAGGCTTGCAGGGAGTTAAAGGCCGCTTTTGCGGGATCG
TCACCCTCAGCAGCGAAAGACAGCATCGGAACGAGGGTAGCAACGGCTACAGAGGCTTTGAGGACTAAAGAC
TTTTTCATGAGGAAGTTTCCATTAAACGGGTAAAATACGTAATGCCACTACGAAGGCACCAACCTAAAACGA
AAGAGGCAAAAGAATACACTAAAACACTCATCTTTGACCCCCAGCGATTATACCAAGCGCGAAACAAAGTAC
AACGGAGATTTGTATCATCGCCTGATAAATTGTGTCGAAATCCGCGACCTGCTCCATGTTACTTAGCCGGAA
CGAGGCGCANACNGTCAATCATAAGGGAACCGAACTGACCAACTTTGAAAGANGACANATGAACGGTGTACA
GACCAGGCGCATANGCTGGCTGACCTTCATCAAGAGTAATCTTGACAAGAACCGGATATTCATTACCCAAAT
CNACGTAANAAAGCTGCTCATTNAGTGAATAAGGCTTGNCCTGANGAGAAACACCAGAACGAGTNGTAAATT
GGGNTTGAGATGTTTNATTTCAACTTTNANNNTTGTGAATTACCTTATGNGATTTTAANNAANTGNCTCATT
NTACNAGTNAGGACGTGGGGAAGAAAANTCTANGTTAANNAAACNANCTAANNNGAANNACANT

The shaded portion of the above sequence is complementary to the following coding sequence: CAG CCT TCG CCT TCT CCT ACG. These codons correspond to the amino acid sequence Glu-Pro-Ser-Pro-Ser-Pro-Thr.

APPENDIX C: Kinetics Work

The results of this study were intended to be used for calibration of a proposed targeted therapeutic construct. The proposed construct consists of a quantum dot conjugated to polyethylene glycol chains with incorporated cleavable peptide linkers. The polyethylene glycol chains conceal a cytotoxic drug. In the presence of matrilysin, the peptide linkers would be cleaved, exposing the cytotoxic drug to nearby cells. Since breast tumors are known to produce matrilysin in high amounts, the conjugated drug would theoretically be preferentially activated in the vicinity of tumors. The results of the study were to assist in calibrating the amount of polyethylene glycol and the amount of drug to conjugate to each quantum dot. Quantitation of matrilysin production has not yet been achieved, but this work evaluated two straightforward approaches and explored several possible reasons for their conflicting results.

Had the results of the activity assay been reliable, they could have been used to calculate matrilysin production per cell in each cell line, using the following equation:

$$\left[\frac{M * \Gamma * (\rho - B)}{\sigma}\right]$$

Where **M** is the molarity to reading ratio, calculated from the peak fluorescence reading of a calibration assay, **Γ** is the moles to grams conversion constant based on the molecular weight of matrilysin, **B** is the average background reading from the plate reader, **ρ** is the well's fluorescence reading, and **σ** is the cell count at the time point corresponding to the well.

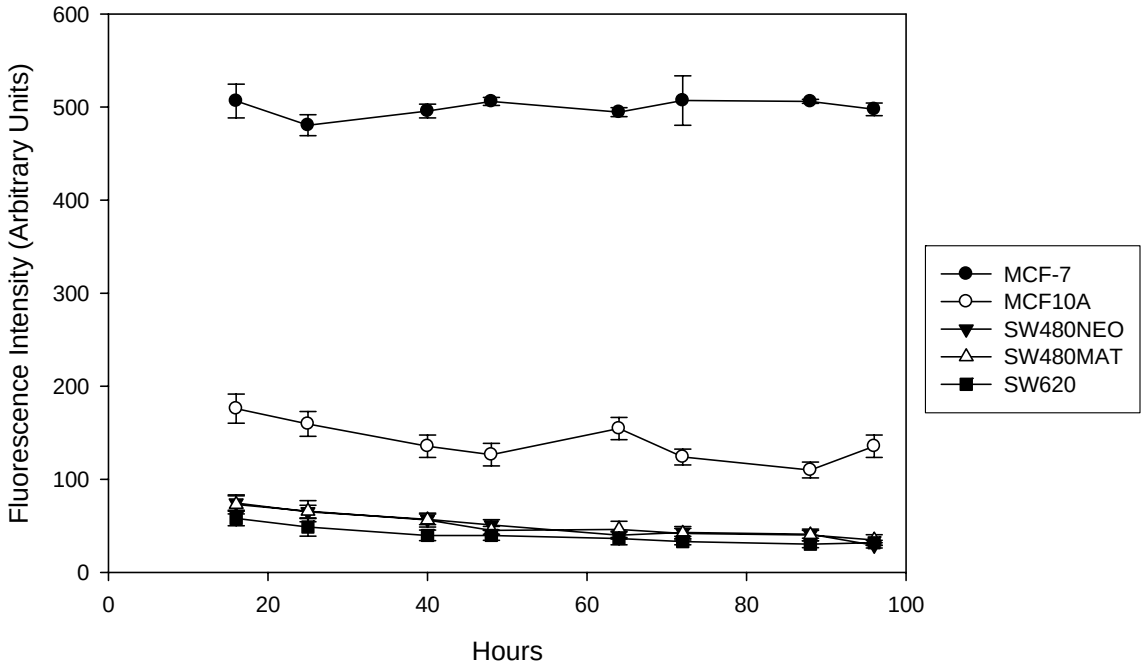

Figure C.1: Fluorescence intensity readings for the matrilysin activity of five tumor cell lines over a 96-hour interval, based on cleavage of a fluorescent substrate designed to be specific for matrilysin.

Fluorescence intensity, an indicator of matrilysin activity, was assessed in five cell lines from 18 to 96 hours after subculture. After subtraction of control fluorescence based on uncleaved substrate, MCF-7 retained a fluorescence activity of approximately 500 units, MCF10A stayed around 150 units, and SW480NEO, SW480MAT, and SW620 cell lines all stayed around 50 units (Figure C.1).

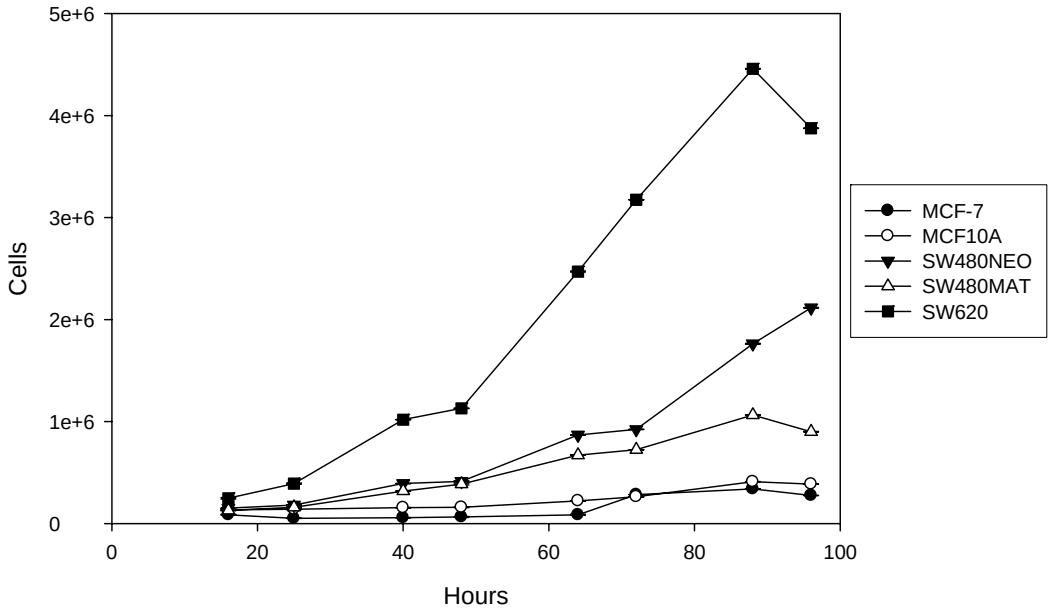

Figure C.2: Representative semi-log growth plot for five cell lines over a 96-hour interval.

At the time of supernatant collection, the cells were detached from the surface of the wells and counted. The cell count data were matched with the fluorescence reading for the corresponding time point to give the data for estimated matrilysin production per cell, as shown in Table C.1 below.

Table C.1: Estimated levels of matrilysin per cell at each time point, in **picograms**, based on fluorescence readings shown in Figure C.1

Time (hours)							
	16	119 ± 9	25 ± 3	9 ± 1	10 ± 2	3.9 ± 0.7	**Color Key**
	25	190 ± 7	21 ± 3	6.1 ± 0.9	8 ± 2	2.3 ± 0.5	MCF-7
	40	177 ± 7	16 ± 2	2.5 ± 0.3	3.3 ± 0.5	0.7 ± 0.1	MCF10A
	48	157 ± 12	14 ± 2	2.1 ± 0.3	2.2 ± 0.3	0.65 ± 0.09	SW480NEO
	64	117 ± 8	13 ± 1	0.75 ± 0.1	1.3 ± 0.2	0.28 ± 0.06	SW480MAT
	72	36 ± 2	8.8 ± 0.7	0.77 ± 0.09	1.1 ± 0.2	0.20 ± 0.02	SW620
	88	30 ± .2	4.9 ± 0.4	0.38 ± 0.05	0.7 ± 0.1	0.13 ± 0.02	
	96	37 ± .5	6.4 ± 0.6	0.21 ± 0.03	0.7 ± 0.1	0.15 ± 0.01	

While the goal of establishing a kinetic, quantitative pattern of matrilysin production by cancer cell lines has not yet been achieved, the work above provides one way in which it could be estimated once reliable data have been obtained.

REFERENCES

1. Acland, G.M., Aguirre, G.D., Bennett, J., *et al.* (2005) "Long-Term Restoration of Rod and Cone Vision by Single Dose rAAV-Mediated Gene Transfer to the Retina in a Canine Model of Childhood Blindness." *Molecular Therapy*, **12**, 1072.

2. Acland, G.M., Aguirre, G.D., Ray, J., *et al.* (2001) "Gene therapy restores vision in a canine model of childhood blindness." *Nat Genet*, **28**, 92.

3. Agnihotri, R., Crawford, H.C., Haro, H., *et al.* (2001) "Osteopontin, a Novel Substrate for Matrix Metalloproteinase-3 (Stromelysin-1) and Matrix Metalloproteinase-7 (Matrilysin)." *J. Biol. Chem.*, **276**, 28261-28267.

4. Parker, A.L., Collins, L., Zhang, X., *et al.* (2005) "Exploration of peptide motifs for potent non-viral gene delivery highly selective for dividing cells." *J Gene Med*, **7**, 1545-1554.

5. Alba, R., Bosch, A. and Chillon, M. (2005) "Gutless adenovirus: last-generation adenovirus for gene therapy." *Gene Therapy*, **12**, S18.

6. Alix-Panabieres, C., Brouillet, J.-P., Fabbro, M., *et al.* (2005) "Characterization and enumeration of cells secreting tumor markers in the peripheral blood of breast cancer patients." *Journal of Immunological Methods*, **299**, 177.

7. Alton, E.W. (2004) "Use of nonviral vectors for cystic fibrosis gene therapy." *Proc Am Thorac Soc*, **1**, 296-301.

8. Atchison DA, Smith G. Optics of the Human Eye. Elsevier. 2000.

9. Ayabe, T., Satchell, D.P., Pesendorfer, P., *et al.* (2002) "Activation of Paneth Cell alpha -Defensins in Mouse Small Intestine." *J. Biol. Chem.*, **277**, 5219-5228.

10. Bachmeier, B.E., Albini, A., Vene, R., *et al.* (2005) "Cell density-dependent regulation of matrix metalloproteinase and TIMP expression in differently tumorigenic breast cancer cell lines." *Exp Cell Res*, **305**, 83-98.

11. Bachmeier, B.E., Vene, R., Iancu, C.M., *et al.* (2005) "Transcriptional control of cell density dependent regulation of matrix metalloproteinase and TIMP expression in breast cancer cell lines." *Thromb Haemost*, **93**, 761-769.

12. Bainbridge, J.W., Mistry, A.R., Thrasher, A.J., *et al.* (2003) "Gene therapy for ocular angiogenesis." *Clin Sci (Lond)*, **104**, 561-575.

13. Bhatia, N., Thiyagarajan, S., Elcheva, I., *et al.* (2006) "GLi2 is targeted for ubiquitination and degradation by beta -TrCP ubiquitin ligase." *J. Biol. Chem.*, M513203200.

14. Binder, C., Hagemann, T., Husen, B., *et al.* (2002) "Relaxin enhances in-vitro invasiveness of breast cancer cell lines by up-regulation of matrix metalloproteases." *Mol Hum Reprod*, **8**, 789-796.

15. Burke, B. (2004) "The role of matrix metalloproteinase 7 in innate immunity." *Immunobiology*, **209**, 51.

16. Busiek, D.F., Ross, F.P., McDonnell, S., *et al.* (1992) "The matrix metalloprotease matrilysin (PUMP) is expressed in developing human mononuclear phagocytes." *J. Biol. Chem.*, **267**, 9087-9092.

17. Campochiaro, P.A. (2002) "Gene therapy for retinal and choroidal diseases." *Expert Opinion on Biological Therapy*, **2**, 537-544.

18. Cavazzana-Calvo, M., Hacein-Bey, S., Basile, G., *et al.* (2000) "Gene Therapy of Human Severe Combined Immunodeficiency (SCID)-X1 Disease." *Science*, **288**, 669-672.

19. Cavazzana-Calvo, M., Lagresle, C., Hacein-Bey-Abina, S., *et al.* (2005) "Gene Therapy for Severe Combined Immunodeficiency." *Annual Review of Medicine*, **56**, 585-602.

20. Chang, E., Miller, J.S., Sun, J., *et al.* (2005) "Protease-activated quantum dot probes." *Biochemical and Biophysical Research Communications*, **334**, 1317.

21. Chevez-Barrios, P., Chintagumpala, M., Mieler, W., *et al.* (2005) "Response of Retinoblastoma With Vitreous Tumor Seeding to Adenovirus-Mediated Delivery of Thymidine Kinase Followed by Ganciclovir." *J Clin Oncol*, **23**, 7927-7935.

22. Chua, G., Lingner, C., Frazer, C., *et al.* (2002) "The sal3+ Gene Encodes an Importin-{beta} Implicated in the Nuclear Import of Cdc25 in Schizosaccharomyces pombe." *Genetics*, **162**, 689-703.

23. Coussens, L.M., Fingleton, B. and Matrisian, L.M. (2002) "Matrix Metalloproteinase Inhibitors and Cancer--Trials and Tribulations." *Science*, **295**, 2387-2392.

24. Crabbe, T., Willenbrock, F., Eaton, D., *et al.* (1992) "Biochemical characterization of matrilysin. Activation conforms to the stepwise mechanisms proposed for other matrix metalloproteinases." *Biochemistry*, **31**, 8500-8507.

25. Crowther, M., Brown, N.J., Bishop, E.T., *et al.* (2001) "Microenvironmental influence on macrophage regulation of angiogenesis in wounds and malignant tumors." *J Leukoc Biol*, **70**, 478-490.

26. Pantarotto, D., Singh, R., McCarthy, D., *et al.* (2004) "Functionalized carbon nanotubes for plasmid DNA gene delivery." *Angew Chem Int Ed Engl*, **43**, 5242-5246.

27. Di Giovine, M., Salone, B., Martina, Y., *et al.* (2001) "Binding Properties, Cell Delivery, and Gene Transfer of Adenoviral Penton Base Displaying Bacteriophage." *Virology*, **282**, 102.

28. Beaujouin, M., Baghdiguian, S., Glondu-Lassis, M., et al. (2006) "Overexpression of both catalytically active and -inactive cathepsin D by cancer cells enhances apoptosis-dependent chemo-sensitivity." *Oncogene*, **25**, 1967-1973.

29. Engelsma, D., Bernad, R., Calafat, J., *et al.* (2004) "Supraphysiological nuclear export signals bind CRM1 independently of RanGTP and arrest at Nup358." *Embo J*, **23**, 3643-3652.

30. Filippov, S., Caras, I., Murray, R., *et al.* (2003) "Matrilysin-dependent Elastolysis by Human Macrophages." *J. Exp. Med.*, **198**, 925-935.

31. Hagemann, T., Robinson, S.C., Schulz, M., *et al.* (2004) "Enhanced invasiveness of breast cancer cell lines upon co-cultivation with macrophages is due to TNF-alpha dependent up-regulation of matrix metalloproteases." *Carcinogenesis*, **25**, 1543-1549.

32. Handsley, M.M. and Edwards, D.R. (2005) "Metalloproteinases and their inhibitors in tumor angiogenesis." *Int J Cancer*, **115**, 849-860.

33. Haro, H., Crawford, H.C., Fingleton, B., *et al.* (2000) "Matrix metalloproteinase-7-dependent release of tumor necrosis factor-alpha in a model of herniated disc resorption." *J Clin Invest*, **105**, 143-150.

34. Harrell, P.C., McCawley, L.J., Fingleton, B., *et al.* (2005) "Proliferative effects of apical, but not basal, matrix metalloproteinase-7 activity in polarized MDCK cells." *Exp Cell Res*, **303**, 308-320.

35. Hulboy, D.L., Rudolph, L.A. and Matrisian, L.M. (1997) "Matrix metalloproteinases as mediators of reproductive function." *Mol. Hum. Reprod.*, **3**, 27-45.

36. Impola, U., Jeskanen, L., Ravanti, L., *et al.* (2005) "Expression of matrix metalloproteinase (MMP)-7 and MMP-13 and loss of MMP-19 and p16 are associated with malignant progression in chronic wounds." *British Journal of Dermatology*, **152**, 720-726.

37. Kehoe, J.W. and Kay, B.K. (2005) "Filamentous phage display in the new millennium." Chem Rev, 105, 4056-4072.

38. Janeway, C.A., Travers, P., Walport, M., Schlomchik, M. Immunobiology: The Immune System in Health and Disease. New York: Garland. 2001.

39. Jaye, D.L., Geigerman, C.M., Fuller, R.E., *et al.* (2004) "Direct fluorochrome labeling of phage display library clones for studying binding specificities: applications in flow cytometry and fluorescence microscopy." *Journal of Immunological Methods*, **295**, 119.

40. Jemal, A., Siegel, R., Ward, E., *et al.* (2006) "Cancer Statistics, 2006." *CA Cancer J Clin*, **56**, 106-130.

41. Jones, L.E., Humphreys, M.J., Campbell, F., *et al.* (2004) "Comprehensive Analysis of Matrix Metalloproteinase and Tissue Inhibitor Expression in Pancreatic Cancer: Increased Expression of Matrix Metalloproteinase-7 Predicts Poor Survival." *Clin Cancer Res*, **10**, 2832-2845.

42. Jun, A.S. and Larkin, D.F. (2003) "Prospects for gene therapy in corneal disease." *Eye*, **17**, 906-911.

43. Laube, B. (2005) "The Expanding Role of Aerosols in Systemic Drug Delivery, Gene Therapy, and Vaccination." *Respiratory Care*, **50**, 1161-1176.

44. Li, Q., Park, P.W., Wilson, C.L., *et al.* (2002) "Matrilysin shedding of syndecan-1 regulates chemokine mobilization and transepithelial efflux of neutrophils in acute lung injury." *Cell*, **111**, 635-646.

45. Liu, X.P., Kawauchi, S., Oga, A., *et al.* (2002) "Prognostic significance of matrix metalloproteinase-7 (MMP-7) expression at the invasive front in gastric carcinoma." *Jpn J Cancer Res*, **93**, 291-295.

46. Lodish, H., Berk, A., Matsudaira, P., Kaiser, C.A., Kreiger, M., Scott, M.P., Zipurksy, S.L., Darnell, J. Molecular Cell Biology. New York: Freeman. 5th Ed. 2004.

47. Ii, M., Yamamoto, H., Adachi, Y., *et al*. (2006) "Role of Matrix Metalloproteinase-7 in Human Cancer Invasion, Apoptosis, Growth, and Angiogenesis." *Exp Biol Med,* 231, 20-27.

48. Martin, K.R. and Quigley, H.A. (2004) "Gene therapy for optic nerve disease." *Eye*, **18**, 1049-1055.

49. Masson, R., Lefebvre, O., Noel, A., *et al.* (1998) "In vivo evidence that the stromelysin-3 metalloproteinase contributes in a paracrine manner to epithelial cell malignancy." *J Cell Biol*, **140**, 1535-1541.

50. McIntyre, J.O., Fingleton, B., Wells, K.S., *et al.* (2004) "Development of a novel fluorogenic proteolytic beacon for in vivo detection and imaging of tumour-associated matrix metalloproteinase-7 activity." *Biochem J*, **377**, 617-628.

51. McIntyre, J.O. and Matrisian, L.M. (2003) "Molecular imaging of proteolytic activity in cancer." *J Cell Biochem*, **90**, 1087-1097.

52. Mendelsohn, J. The molecular basis of cancer. Philadelphia: Saunders. 2nd. 2001.

53. Miyazaki, K., Koshikawa, N., Hasegawa, S., *et al.* (1999) "Matrilysin as a target for chemotherapy for colon cancer: use of antisense oligonucleotides as antimetastatic agents." *Cancer Chemother Pharmacol*, **43 Suppl**, S52-55.

54. Mohan, R.R., Sharma, A., Netto, M.V., *et al.* (2005) "Gene therapy in the cornea." *Prog Retin Eye Res*, **24**, 537-559.

55. Momiyama, N., Koshikawa, N., Ishikawa, T., *et al.* (1998) "Inhibitory effect of matrilysin antisense oligonucleotides on human colon cancer cell invasion in vitro." *Mol Carcinog*, **22**, 57-63.

56. Beaujouin, M., Baghdiguian, S., Glondu-Lassis, M., et al. (2006) "Cathepsin D: newly discovered functions of a long-standing aspartic protease in cancer and apoptosis" *Cancer Letters*, **237**, 167-179.

57. Mori, K., Gehlbach, P., Ando, A., *et al.* (2002) "Regression of ocular neovascularization in response to increased expression of pigment epithelium-derived factor." *Invest Ophthalmol Vis Sci*, **43**, 2428-2434.

58. Mullis, K.B. (1988) "Primer-directed enzymatic amplification of DNA with a thermostable DNA polymerase." *Science*, **239**, 487-491.

59. Myelona E, K.A., Mavrommatis J, Markaki S, Keramopoulos A, Nakopoulou L. (2005) "The Multifunctional Role of the Immunohistochemical expression of MMP-7 in Breast Cancer." *APMIS*, **113**, 246-255.

60. Nakamura, M., Miyamoto, S.i., Maeda, H., *et al.* (2005) "Matrix metalloproteinase-7 degrades all insulin-like growth factor binding proteins and facilitates insulin-like growth factor bioavailability." *Biochemical and Biophysical Research Communications*, **333**, 1011.

61. Nemori, R., Yamamoto, M., Kataoka, F., *et al.* (2005) "Development of In Situ Zymography to Localize Active Matrix Metalloproteinase-7 (Matrilysin-1)." *J. Histochem. Cytochem.*, jhc.5A6631.2005.

62. Newell, K.J., Matrisian, L.M. and Driman, D.K. (2002) "Matrilysin (matrix metalloproteinase-7) expression in ulcerative colitis-related tumorigenesis." *Mol Carcinog*, **34**, 59-63.

63. Nishizuka, I., Ichikawa, Y., Ishikawa, T., *et al.* (2001) "Matrilysin stimulates DNA synthesis of cultured vascular endothelial cells and induces angiogenesis in vivo." *Cancer Lett*, **173**, 175-182.

64. Pacheco, M.M., Mourao, M., Mantovani, E.B., *et al.* (1998) "Expression of gelatinases A and B, stromelysin-3 and matrilysin genes in breast carcinomas: clinico-pathological correlations." *Clin Exp Metastasis*, **16**, 577-585.

65. Pang, J.-j., Chang, B., Kumar, A., *et al.* (2005) "Gene Therapy Restores Vision-Dependent Behavior as Well as Retinal Structure and Function in a Mouse Model of RPE65 Leber Congenital Amaurosis." *Molecular Therapy*, **In Press, Corrected Proof**,

66. Puerta, D.T., Lewis, J.A. and Cohen, S.M. (2004) "New beginnings for matrix metalloproteinase inhibitors: identification of high-affinity zinc-binding groups." *J Am Chem Soc*, **126**, 8388-8389.

67. Ralph, G.S., Binley, K., Wong, L.F., *et al.* (2006) "Gene therapy for neurodegenerative and ocular diseases using lentiviral vectors." *Clin Sci (Lond)*, **110**, 37-46.

68. Rasmussen, H., Chu, K.W., Campochiaro, P., *et al.* (2001) "Clinical protocol. An open-label, phase I, single administration, dose-escalation study of ADGVPEDF.11D (ADPEDF) in neovascular age-related macular degeneration (AMD)." *Hum Gene Ther*, **12**, 2029-2032.

69. Rhee, M. and Davis, P.B. (2005) "Mechanism of uptake of C105Y-a novel cell penetrating peptide." *J Biol Chem*,

70. Rubanyi, G.M. (2001) "The future of human gene therapy." *Mol Aspects Med*, **22**, 113-142.

71. Salmela, M.T., Pender, S.L., Karjalainen-Lindsberg, M.L., *et al.* (2004) "Collagenase-1 (MMP-1), matrilysin-1 (MMP-7), and stromelysin-2 (MMP-10) are expressed by migrating enterocytes during intestinal wound healing." *Scand J Gastroenterol*, **39**, 1095-1104.

72. Shiomi, T. and Okada, Y. (2003) "MT1-MMP and MMP-7 in invasion and metastasis of human cancers." *Cancer Metastasis Rev*, **22**, 145-152.

73. Shirafuji, Y., Tanabe, H., Satchell, D.P., *et al.* (2003) "Structural Determinants of Procryptdin Recognition and Cleavage by Matrix Metalloproteinase-7." *J. Biol. Chem.*, **278**, 7910-7919.

74. Snoek-van-Beurden, P.A.M. and Von den Hoff, J.W. (2005) "Zymographic techniques for the analysis of matrix metalloproteinase and their inhibitors." *Biotechniques*, **38**, 73-83.

75. Somerville, R.P., Oblander, S.A. and Apte, S.S. (2003) "Matrix metalloproteinases: old dogs with new tricks." *Genome Biol*, **4**, 216.

76. Soule, H.D., Maloney, T.M., Wolman, S.R., *et al.* (1990) "Isolation and characterization of a spontaneously immortalized human breast epithelial cell line, MCF-10." *Cancer Res*, **50**, 6075-6086.

77. Srivastava, A. (2005) "Hematopoietic Stem Cell Transduction by Recombinant Adeno-Associated Virus Vectors: Problems and Solutions." *Hum Gene Ther*,

78. Surendran, K., Simon, T.C., Liapis, H., *et al.* (2004) "Matrilysin (MMP-7) expression in renal tubular damage: association with Wnt4." *Kidney Int*, **65**, 2212-2222.

79. Vargo-Gogola, T., Crawford, H.C., Fingleton, B., *et al.* (2002) "Identification of novel matrix metalloproteinase-7 (matrilysin) cleavage sites in murine and human Fas ligand." *Arch Biochem Biophys*, **408**, 155-161.

80. Vargo-Gogola, T., Fingleton, B., Crawford, H.C., *et al.* (2002) "Matrilysin (matrix metalloproteinase-7) selects for apoptosis-resistant mammary cells in vivo." *Cancer Res*, **62**, 5559-5563.

81. Wagenaar-Miller, R.A., Gorden, L. and Matrisian, L.M. (2004) "Matrix metalloproteinases in colorectal cancer: is it worth talking about?" *Cancer Metastasis Rev*, **23**, 119-135.

82. Wang, F., Reierstad, S. and Fishman, D.A. (2005) "Matrilysin over-expression in MCF-7 cells enhances cellular invasiveness and pro-gelatinase activation." *Cancer Letters*, **In Press, Corrected Proof**.

83. Wang, F.Q., So, J., Reierstad, S., *et al.* (2005) "Matrilysin (MMP-7) promotes invasion of ovarian cancer cells by activation of progelatinase." *Int J Cancer*, **114**, 19-31.

84. Pan, W.H. and Clawson, G.A. (2006) "Antisense applications for biological control." *J Cell Biochem*, **98**, 14-35.

85. Wielockx, B., Libert, C. and Wilson, C. (2004) "Matrilysin (matrix metalloproteinase-7): a new promising drug target in cancer and inflammation?" *Cytokine & Growth Factor Reviews*, **15**, 111.

86. Wilson, C.L. and Matrisian, L.M. (1996) "Matrilysin: an epithelial matrix metalloproteinase with potentially novel functions." *Int J Biochem Cell Biol*, **28**, 123-136.

87. Wilson, C.L., Ouellette, A.J., Satchell, D.P., *et al.* (1999) "Regulation of Intestinal -Defensin Activation by the Metalloproteinase Matrilysin in Innate Host Defense." *Science*, **286**, 113-117.

88. Wilson, J.M. (2004) "Adeno-associated Virus and Lentivirus Pseudotypes for Lung-directed Gene Therapy." *Proc Am Thorac Soc*, **1**, 309-314.

89. Woessner, J.F., Jr. (1991) "Matrix metalloproteinases and their inhibitors in connective tissue remodeling." *Faseb J*, **5**, 2145-2154.

90. Woessner, J.F., Jr. and Nagase, H. Matrix Metallproteinases and TIMPs. Oxford University Press. 2000.

91. Wolf, C., Rouyer, N., Lutz, Y., *et al.* (1993) "Stromelysin 3 belongs to a subgroup of proteinases expressed in breast carcinoma fibroblastic cells and possibly implicated in tumor progression." *Proc Natl Acad Sci U S A*, **90**, 1843-1847.

92. Yu, W.H., Woessner, J.F., Jr., McNeish, J.D., *et al.* (2002) "CD44 anchors the assembly of matrilysin/MMP-7 with heparin-binding epidermal growth factor precursor and ErbB4 and regulates female reproductive organ remodeling." *Genes Dev*, **16**, 307-323.

93. Zucker, S. and Vacirca, J. (2004) "Role of matrix metalloproteinases (MMPs) in colorectal cancer." *Cancer Metastasis Rev*, **23**, 101-117.

94. Aston-Weiner, Ashley. (2003) Differential phage display for discovery of nuclear localization peptides: application to mammary adenocarcinoma. Master's Thesis. Vanderbilt University.

95. Seiler, N., Schneider, Y., Gosse, F., *et al.* (2004) "Polyploidisation of metastatic colon carcinoma cells by microtubule and tubulin interacting drugs: effect on proteolytic activity and invasiveness." *Int J Oncol*, **25**, 1039-1048.